AEROSPACE ENGINEERING
Bioastronautics and
Human Performance

# SmartSuit: Hybrid, Intelligent, and Highly Mobile EVA Spacesuit for Next Generation Exploration Missions

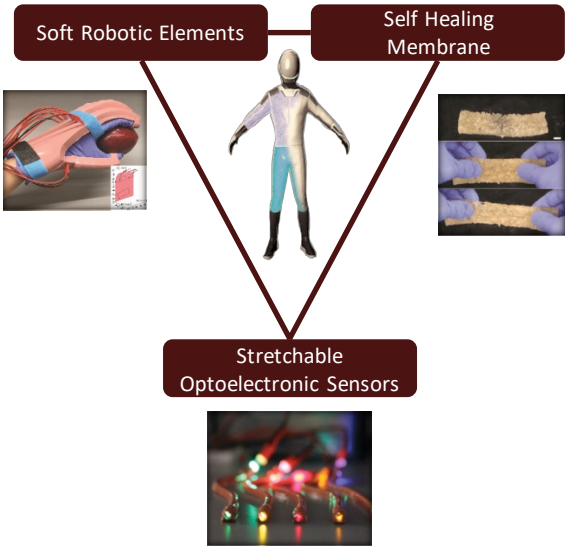


## NASA Innovative Advance Concepts (NIAC)

## Phase I Final Report

Dr. Ana Diaz-Artiles[1] (PI)
Dr. Robert Shepherd[2], Ph.D. (Co-I)
Logan Kluis[1]
Nathan Keller[3]
Hedan Bai[2]
Narahari Iyengar[2]
Chase Audirsch[1]

[1]Aerospace Engineering Department, Texas Engineering Experiment Station
[2]Sibley School of Mechanical and Aerospace Engineering, Cornell University
[3]Health and Kinesiology Department, Texas A&M University

March 9th 2020

This page intentionally left blank.

## Executive Summary

The "SmartSuit" is a novel spacesuit intelligent architecture for extravehicular activity (EVA) operations on Mars and other planetary environments that increases human performance by an order of magnitude on several quantifiable fronts for exploration missions. The SmartSuit spacesuit, while gas-pressurized, also incorporates soft-robotics technology that allows astronauts to be highly mobile and better interact with their surroundings. The spacesuit also incorporates a soft and stretchable self-healing skin (or membrane) located in the outer layer that not only protects the astronaut but also collects data through integrated, transparent sensors embedded in the membrane. These sensors are capable of visually displaying environmental and membrane structural information, providing visual feedback to the wearer about the surroundings and suit integrity.

The hybrid and intelligent spacesuit proposed is designed with the philosophy of enhancing motion and dexterity, reparability, and sensor integration to interact with the surroundings and detect spacesuit damage. The proposed hybrid technology, i.e., adding full-body soft-robotic elements to the gas-pressurized spacesuit, will enable enhanced dexterity, increased comfort, and a feeling of normalcy to facilitate both scientific and exploration operations on planetary missions like those expected on Mars' surface. Additionally, the soft-robotic layer has the potential to provide mechanical counterpressure (MCP) to the wearer, which would allow a decrease in the gas-operating pressure within the suit, therefore further enhancing suit mobility. We expect the proposed spacesuit technology to also reduce the numerous spacesuit-fit injuries and discomfort experienced by present astronauts due to the current highly pressurized spacesuits with no robotic assistance. Our proposed spacesuit significantly improves on the state-of-the-art in spacesuit design, addressing many issues in surface mobility, reparability and re-usability, safety, EVA preparation time, EVA duration time, and both physical and psychological fatigue.

During Phase I, we have investigated our spacesuit concept in the context of the current Mars Design Reference Mission 5.0. In particular, we have conducted a comprehensive human performance analysis in the context of planetary EVAs and have quantified the benefits of our SmartSuit in terms of mobility, metabolic needs, and EVA preparation time related to prebreathing requirements. Additionally, we have investigated soft-robotic actuator concepts, self-healing membrane formulations, and optoelectronic sensor architectures; and have identified promising candidates of these technologies for SmartSuit. We have built two soft-robotic knee actuator prototypes, as well as a preliminary self-healing membrane with optoelectronic sensors embedded in it that are capable of recovering full functionality after severe damage (i.e. deep cut through the membrane/sensor system with a knife). Overall, the phase I efforts have advanced our proposed concept from TRL 1 to TRL2.

## Acknowledgments

The authors gratefully acknowledge support from NASA, in particular the NIAC program office, as well as helpful feedback and constructive criticisms from the NIAC community and colleagues in academia and industry. We would also like to acknowledge Darren Hartl and Rodney Inmon for their advice and support in designing and executing our actuator testing.

# Table of Contents

# 1 Introduction, Proposed Concept, and Scope

Current gas-pressurized spacesuits, such as the Extravehicular Mobility Unit (EMU), cause additional fatigue, injuries (1, 2, 10, 11, 16, 21, 22, 25, 28, 32, 33, 40), and are metabolically expensive (6, 7, 23) during extravehicular activities (EVAs). They also allow for limited interaction with the environment and punctures in the suit may result in catastrophic failures. We propose a novel spacesuit intelligent architecture for EVA operations on Mars and other planetary environments that increases human performance by an order of magnitude on several quantifiable fronts for exploration missions.

The SmartSuit, our advanced planetary spacesuit concept, makes use of three technological innovations to negate the shortcomings of current spacesuits:

1. Full body soft-robotic layer within the gas-pressurized suit to enhance mobility.
   - This layer also provides mechanical counterpressure, allowing reduction in gas-operating pressure, further increasing mobility.
2. An outer layer made of stretchable self-healing skin to enhance safety.
3. Stretchable integrated optoelectronic sensors embedded in the membrane to enhance interaction with the environment and monitor skin membrane structural health data,

We envision that SmartSuit will enhance human performance in multiple fronts:

- Mobility and comfort
- Reusability, Reparability and Safety
- EVA preparation and Duration time

The main contributions and highlights in Phase I include:

- Comprehensive human-spacesuit interaction and biomechanical analysis of the SmartSuit concept during walking, including a detailed analysis of the impact on human performance in the context of metabolic expenditure.
- Initial prototyping and testing of two soft-robotic knee actuators
- Tradespace exploration of benefits of the level of mechanical counterpressure provided by the soft-robotic layer: impacts on pre-breathing time, mobility, and human performance.
- Tradespace exploration and characterization of mechanical properties of self-healing materials and optoelectronic sensors in the context of the SmartSuit. Identification of suitable candidates.
- Concept of Operations and overall benefit in the context of a human mission to Mars.

In the following sections, we provide additional details of each one of these contributions, beginning with framing the proposed concept within the existing literature.

# 2 Background

## 2.1 Spacesuits for Extravehicular Activity: Injuries and Overall Human Performance

Extravehicular Activity (EVA) is one of the most challenging activities that astronauts need to perform in space. NASA's current gas-pressurized spacesuit, the Extravehicular Mobility Unit (EMU), is a ΔP=29.6 KPa (4.3 psi), 100% oxygen spacesuit made of 14 different layers (20). The EMU is used in a microgravity environment, and it has not been designed to operate in different conditions such as planetary surfaces. Conversely, the Mark III gas-pressurized spacesuit technology demonstrator was developed for EVAs on the moon and Mars, providing a better mobility range to facilitate planetary exploration. However, all gas-pressurized spacesuits still require astronauts to use their strength to move the suit, which can be fatiguing and significantly affect the metabolic cost of human movement and locomotion (6, 7, 23). The current EMU spacesuit causes many astronauts minor musculoskeletal injuries and discomfort, which could lead to suboptimal EVA performance and could impact mission success (10, 25, 28, 32, 33, 40). In particular, hand injuries are the most common injuries both in training and in-flight (3, 12, 17). They are due in part to the axial force applied to fingers in order to move the pressurized and stiff gloves (9). Injuries also occur due to the finger pad pressure needed to articulate the gloves (10), and the presence of moisture in the gloves also exacerbates the onset of hand injuries (9). As a consequence, astronauts may develop fingernail delamination, or onycholysis after an EVA.

In this context, we propose to introduce soft-robotic technology to increase human performance during EVA. This brings two essential benefits. On one hand, mobility within the spacesuit is highly improved, allowing for full range of movements while performing an EVA, including hand movement. Also, surface displacements are more efficient, and the optoelectronic technology embedded in the membrane allows for an enhanced interaction with the environment during the EVA traverses, and for example permits astronauts to interact with and "feel" rocks directly during a sampling traverse when exploring the Mars surface. This enhanced interaction during traverses also enables more crew autonomy and facilitates in-situ decision making. Additionally, the mechanical counterpressure generated by the soft-robotic layer reduces pre-breathing times, which currently can last up to four hours and therefore entail a large waste of mission resources (i.e. astronaut time) (36). All in all, EVA times can be drastically reduced through all phases of EVA: pre-breathing, transportation to worksite, and worksite operations.

## 2.2 Soft-Robotic Exoskeletons to Enhance Human Performance

Robotic elements or exoskeletons can greatly enhance human performance during surface exploration. However, most of the current exoskeletons being developed are composed of hard robotic elements that can cause contact injuries to the wearer and also make their potential integration with a spacesuit extremely challenging. Instead, we propose to use soft-robotic technology with highly compliant robotic elements to facilitate human-spacesuit interactions (27, 37). From the myriad potential uses of soft robotics, wearable systems are one of the most attractive. Further, the use of compressed gases for pressurization in spacesuits means little extra complexity needs to be added for operation of fluidically actuated soft robotic elements. Due to

the low stiffness and conformability of soft robotic systems, we have applied these actuators and sensors as force augmenting human interfaces for SmartSuit.

In previous efforts, Co-I Prof. Shepherd developed a robotic glove with integrated optical strain sensors and EMG control to increase the grasping force of the wearer. This pneumatically-actuated glove had embedded stretchable sensors and an electromyographic bionic arm interface for muscle activated grasping and closed-loop feedback control over grasping position (42, 43) (see **Figure 1**). The body of the glove is made of a silicone elastomer (ELASTOSIL M4601 A/B; Wacker Chemie AG) combined with 10% silicone thinner, and each finger has a series of interconnected air chambers and nylon fabric along the palm side of each finger, so upon fluid pressurization, the actuators cause a grasping motion. Actuator motion analysis using conventional composite beam theory (for more details (43)) yields a maximum net finger moment:

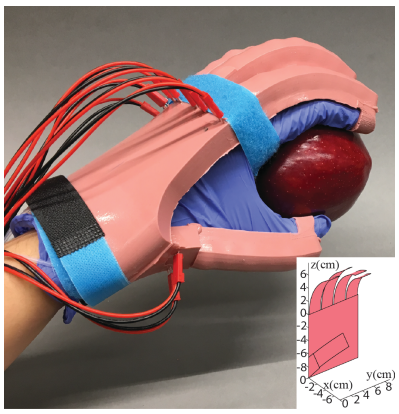


**Figure 1**: Soft-robotic glove (42, 43)

$$M_{N_{max}} = \pi r^3 \Delta p$$

where r is the radius of the finger and $\Delta p$ is the pressure of the pneumatic fluid. In our previous efforts, we used $\Delta p$= 270 KPa and r=10 mm, which yields a soft-robotic induced moment of $M_{N_{max}} = 0.8\ Nm$. (for a 8-cm-long finger this yields a theoretical upper limit for the finger force of 10N). Experimental data using this device showed that the soft-robotic glove augmented the finger force by a factor of 1.6 (43).

# 3 SmartSuit Design and Analysis

## 3.1 Soft-Robotic Elements within the Spacesuit

### 3.1.1 Reduction of Spacesuit Joint-Torques – Biomechanical Analysis and Impacts on Human Performance

We conducted biomechanical simulations to study the impact on human joint torques, muscle forces, and metabolic expenditure while: (i, EMU conditions) wearing the current EMU spacesuit and, (ii, SmartSuit conditions) when assisted by our proposed soft-robotic components in multiple joints to enhance and facilitate joint motion during planetary surface exploration.

#### *3.1.1.1 Modeling Spacesuit Torques*

Currently, astronauts using the EMU spacesuit have to work against the suit to bend any of the extremities. Thus, from the biomechanical point of view, we can model the effect of the suit as external torques applied to the human body based on experimental spacesuit torque-angle relationships. In the current EMU spacesuit, torque-angle relationship from different joints were measured using an instrumented robot inside a spacesuit (12, 29). Some of the lower extremity joint-torque relationships (ankle flexion, knee flexion, hip flexion, and hip abduction) are shown in **Figure 2** below. We focused on hip, knee, and ankle joints since these are the joints that are directly involved in walking (expected for astronauts exploring the surface of Mars).

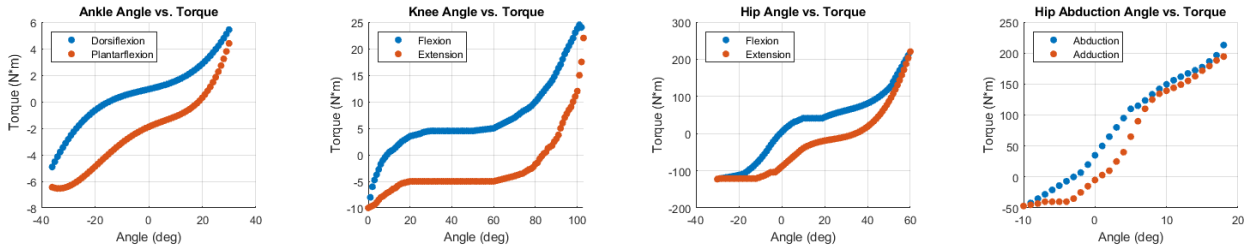


**Figure 2**: Joint-torque relationships for the ExtraVehicular Mobility Unit (EMU) spacesuit. Joints-torques included in our biomechanical simulations include Ankle Dorsiflexion/Plantarflexion, Knee Flexion/Extension, Hip Flexion/Extension, and Hip Abduction/Adduction. Data taken from (29).

For example, the EMU knee flexion/extension torque as a function of the knee angle (α) is shown in **Figure 2b**. The initial position corresponds to α = 0 degrees, located at the bottom left of the figure. In this position, the leg is entirely extended such that the thigh and the shank are completely aligned. The upper blue line represents the spacesuit torques corresponding to different knee angles from 0-100 degrees during knee flexion motion. At the point of maximum knee flexion corresponding to α = 100 degrees, the torque induced by the EMU is 25 Nm. On the other hand, the bottom orange line represents the EMU torques corresponding to knee angles from 100 to 0 degrees during knee extension motion. All graphics show a hysteretic behavior that is characteristic of highly pressurized spacesuits.

Thus, based on the EMU joint-torque relationships, we have conducted an exhaustive biomechanical analysis (described below, see additional details here (9)) to calculate astronaut

joint torques, muscle forces, and metabolic consumption during a walking motion in unsuited and suited (EMU) planetary exploration scenarios. We analyzed one gait cycle (from 0% to 100% of movement), which included the following phases: mid-swing, initial contact, loading response, mid-stance, terminal stance, initial swing, and back mid-swing. These results provide specific quantitative decrements on numerous biomechanical and human performance parameters due to the presence of the EMU spacesuit.

In our SmartSuit spacesuit concept, we envision the use of soft-robotic actuators on the most relevant joints to counteract the spacesuit-induced torques and thus, facilitate movement. Based on our previous experience with soft-robotic actuators as well as based on the theoretical framework described above (see further details in the following paragraphs about our actuator prototypes), we expected > 10 Nm of assistive torque generated in each joint (which we also verified with our prototypes, see paragraph 3.1.2.2). Thus, we also conducted similar biomechanical analysis to simulate the SmartSuit condition, which included the presence of these soft-robotic actuators while wearing the gas-pressurized EMU spacesuit.

#### *3.1.1.2 Biomechanical Analysis Framework to Investigate Human-Spacesuit Interaction*

To conduct our biomechanical analysis we used OpenSim, an open-source biomechanical software (8) that offers various analysis capabilities such as inverse kinematics (IK), inverse dynamics (ID), residual reduction algorithm (RRA) (18), computed muscle control (CMC) (34, 35), and metabolic probing (30). A large community of researchers have used this to model a variety motions consisting of walking (4, 31), running (14), jumping (3), and squatting (13), and many other publications have attested the myriad of features that Openim has to offer (5, 26).

Our model for simulations was created by Delp in 1990 [13] but has undergone several iterations to improve reliability. The fictitious astronaut model has a height of 1.8m, a mass of 75 Kg, and is represented in **Figure 3**. The model does not include upper body appendages but contains a relatively precise model of the lower body bones and muscles, which make the model appropriate for walking simulations. It comprises 54 linear muscle actuators, represented by the red lines of action, and it has 23 degrees of freedom. The 12 segments included in the model are: one “Torso” (includes head), one “Pelvis”, two “Femur”, two “Tibia”, two “Talus”, two “Calcaneus”, and two “Toes”. The 23 degrees include three rigid body translations and three rigid body rotations with respect to the ground frame, three lumbar coordinates (extension, bending, and rotation), and 14 (7 per leg) lower body coordinates (hip flexion, hip adduction, knee flexion, ankle flexion, subtalar motion, and metatarsophalangeal motion).

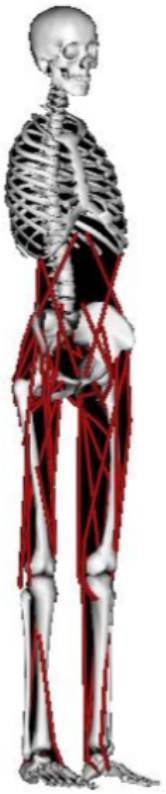

**Figure 3**: Human Model

Our biomechanical analysis included multiple steps, and a flow chart of the computational procedure to simulate motions is displayed in **Figure 4** (see legend for additional details of all the different steps). We used available motion capture data of a walking gait cycle of a generic subject represented by the model already described in **Figure 3**. The following steps included IK (to calculate joint angles and position), ID (to calculate joint torques), RRA (to improve the dynamic consistency of the simulation), CMC (to calculate a set of muscle activations and forces) and metabolic calculations. The metabolic model used was developed and validated by Umberger in 2010 (38, 39) and accounts for metabolic contributions from different factors, including heat rate dynamics (based on percent of fast twitch muscle fibers, percentage of total muscle activation, speed of the muscle shortening or lengthening, and the efficiency of both for slow twitch and fast twitch muscle fibers), and mechanical work.

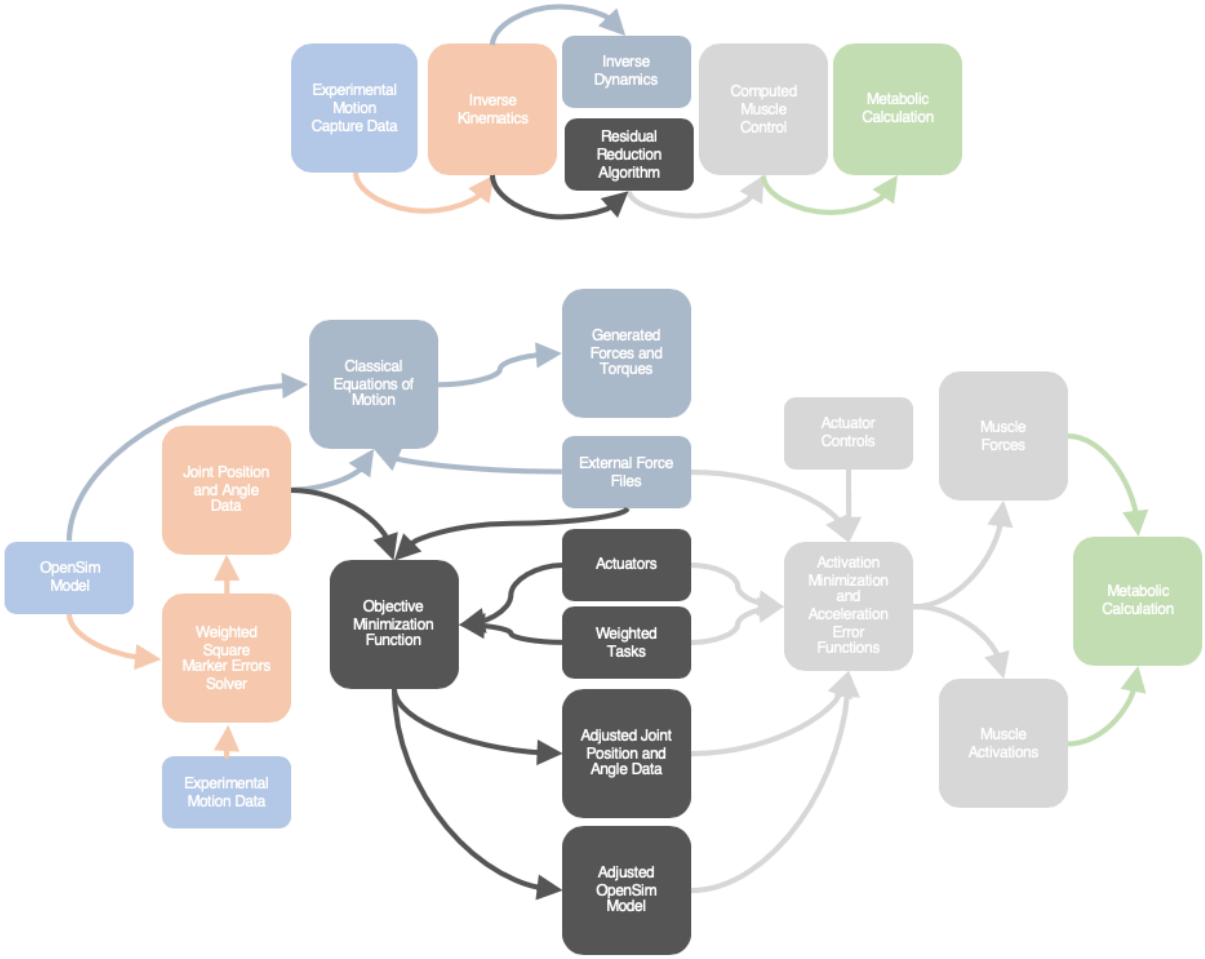


**Figure 4**: The overall computational procedure using OpenSim is summarized above. Experimental Motion Capture data relates to the experimental data collected from tests or studies (we used already existing walking data available in OpenSim). Inverse Kinematics computes the joint angles and positions of the human model based on the experimental motion capture data. Inverse Dynamics solves for the forces and torques of the different bodies and joints in the human model. The Residual Reduction Algorithm slightly adjusts the center of mass of the model and associated kinematics to improve dynamic consistency. The CMC tool computes a set of muscle activations and forces that drives the dynamic model to track the desired kinematics. Finally, muscle and actuator activation data are then used by the Metabolic Calculator to find the total energy expenditure for the specific motion being analyzed.

To simulate EMU suited conditions, EMU torque data were incorporated into the simulations as external torques based on the experimental torque-angle relationships described in **Figure 2**. The specific joint angles and associated EMU spacesuit torques implemented during the gait simulations are depicted in **Figure 5**. In the case of the SmartSuit conditions, soft-robotic actuator torques were combined with EMU torques, then incorporated into the simulations.

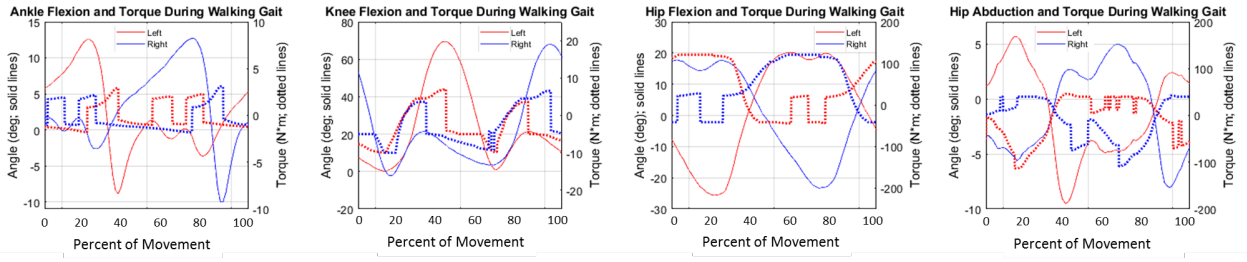


**Figure 5**: Joint angles (solid lines: lef (red) and right (blue) legs) and associated EMU spacesuit torques (dotted lines) during a gait cycle.

### *3.1.1.3 Results and Impacts on Human Performance*

As an example of some of our analyses conducted, **Figure 6** below shows knee joint angles (inverse kinematics, left graph) and knee joint torques (inverse dynamics, right graph) during the walking motion analyzed (one single gait cycle as described above):

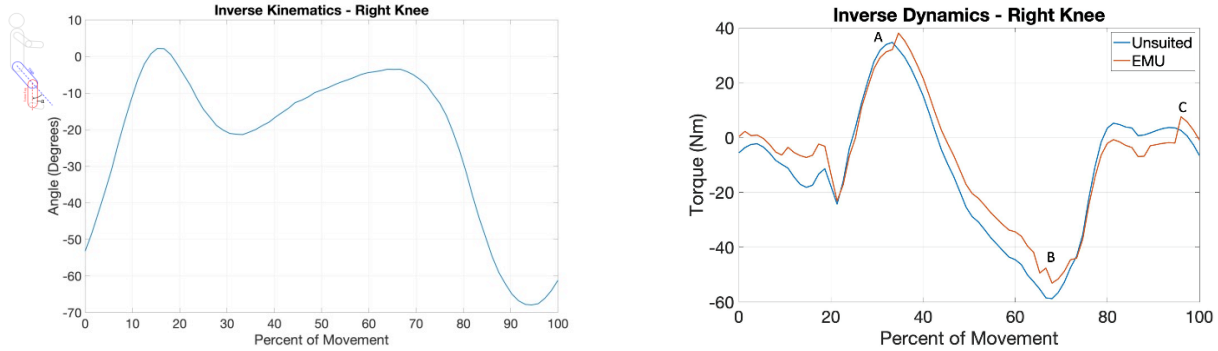


**Figure 6:** Left) Inverse Kinematic results (i.e. joint angle vs. time) of the right knee angle during a gait cycle. Right) Inverse Dynamics results (i.e. joint torque vs. time) of the right knee during a gait cycle in unsuited and suited (EMU) conditions. Notable regions in the gait cycle include: A) initiation of right foot single support stage, B) terminal stance phase, and C) Initial swing phase.

The inverse dynamic results (**Figure 6**, right) highlights the difference in right knee joint torque due to the presence of the EMU during walking.

**Figure 7** below shows the total right knee extension force (left graph) and the total right ankle dorsiflexion force (right graph) generated during one gait cycle. Results suggest that the total force exerted by knee extensors and ankle dorsiflexors is lower in the SmartSuit vs. EMU conditions. Thus, during walking, the presence of the EMU elicits a higher engagement of the knee extensors (**Figure 7** left) to overcome the presence of the spacesuit-induced force. However, the presence of soft-robotic actuators in the SmartSuit provides additional torque to overcome some of these efforts resulting in a lower overall force required by the knee extensors. In the case of dorsiflexion (**Figure 7** right), the SmartSuit actuators are also able to counteract the force generated in unsuited conditions.

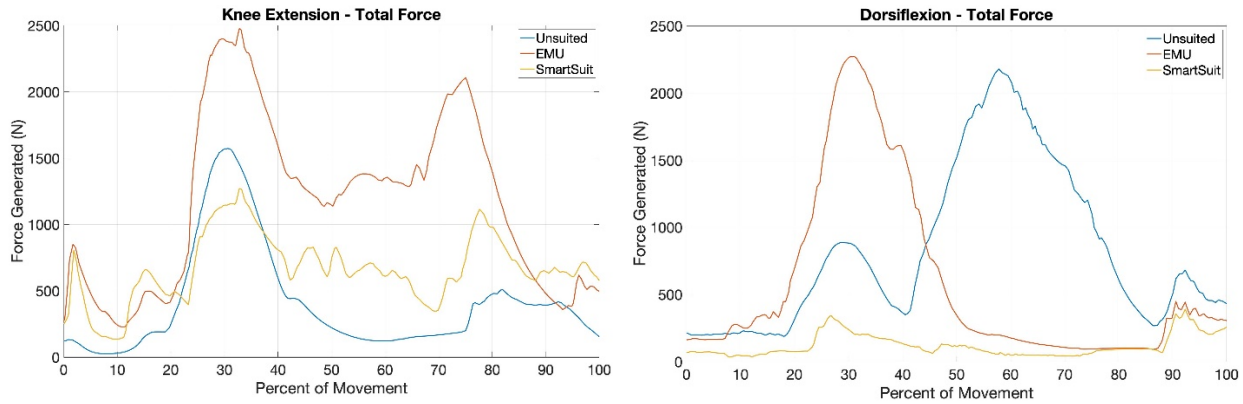


**Figure 7:** Left) Right knee total extension force (including rectus femoris and vastus intermedialis muscle) during a gait cycle. Right) Total dorsiflexion force (tibialis anterior) during a gait cycle.

This lower effort in multiple extremities due to the presence of the soft-robotic actuators translates into an overall lower metabolic consumption when wearing our SmartSuit concept. Metabolic results of the entire body during a gait cycle are shown in **Figure 8.** The total increase in metabolic consumption from EMU torques is approximately 66% with respect to normal walking in unsuited conditions. **The soft-robotic actuators reduce the total metabolic cost by 15% for the same walking motion.**

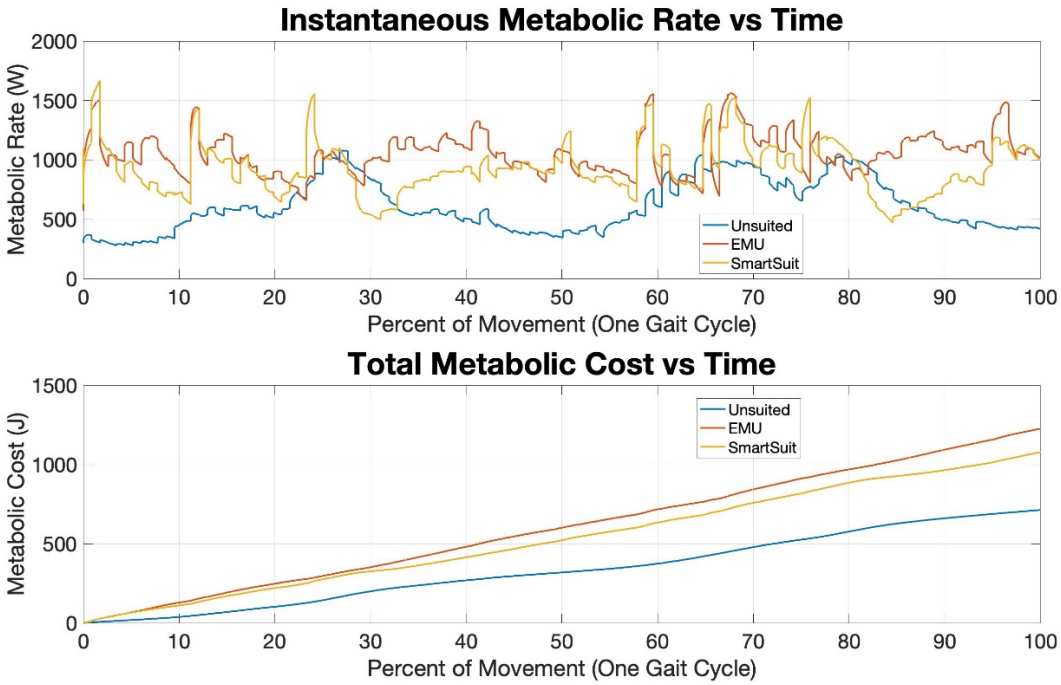


**Figure 8:** Instantaneous metabolic rate (top) and total metabolic cost over time (bottom) for one gait cycle for the three conditions investigated: unsuited, EMU, and SmartSuit.

**Table 1** below provides metabolic data in terms of kilocalories needed to walk in unsuited and suited conditions. The first two columns specify the energy needed during one gait cycle based on our simulations. The 3rd and 4th columns specify the metabolic energy as a function of time, assuming that 1 gait cycle is completed in 1.1 seconds. According to our simulations, the **SmartSuit can save ~120 Kilocalories per hour during a planetary EVA with respect to the EMU**.

**Table 1**: Caloric rates in different unit are provided for unsuited and suited (EMU and SmartSuit conditions). One gait cycle is assumed to be completed in 1.1 seconds (as it was in our biomechanical simulations)

| Condition | Joules per Gait Cycle | Kilocalories per Gait Cycle | Kilocalories per Second | Kilocalories per Hour |
|---|---|---|---|---|
| Unsuited | 713 | 0.170 | 0.155 | 556 |
| EMU | 1226 | 0.293 | 0.266 | 957 |
| SmartSuit | 1077 | 0.257 | 0.234 | 842 |

During a realistic EVA on the surface of Mars, we expect astronauts to explore and interact with the environment and perform motions other than walking (e.g. bending and picking rocks from the ground). Future work includes the use more realistic human models (i.e. model with arms) and expand these biomechanical and metabolic analyses to additional tasks and motions (e.g. squatting to pick up and object from the ground) to investigate more realistic operational scenarios from the Mars Design Reference Mission 5.0.

## 3.1.2 Soft Robotic Joint Actuator Prototypes – Initial Testing & Characterization

### *3.1.2.1 Actuator Design*

We have designed and built two knee soft-robotic actuator prototypes made via direct Digital Light Synthesis (DLS) 3D printing of polyurethane (EPU 40, Carbon 3D Incorporated), shown in **Figure 10** and **Figure 13**. These actuators are designed to counteract spacesuit joint torques to improve mobility and metabolic expenditures on EVA missions. They are actuated by compressed air and can produce a bending motion to assist in the movements of the wearer. Our two designs were made and tested to optimize the "pressure input - torque output" relationship in the actuator. The purpose of doing so is to obtain the maximum possible torque while minimizing the pressure required to actuate.

The first prototype, shown in **Figure 10**, has a series of interconnected hollow chambers through a strain-limiting layer along the knee side. Upon fluid pressurization, the actuator causes a bending motion. In the context of beam theory, the neutral axis for bending is just outside of the strain-limiting fabric and not in the middle of the actuator.

**Figure 9**: Knee soft-robotic actuator prototype #1 with integrated strain-limiting layer: isometric view (left) and front view (right). The chambers are connected internally through the strain-limiting layer.

**Figure 10** and **Figure 11** show the knee actuator prototype #1 in unpressurized (resting state) and pressurized configurations.

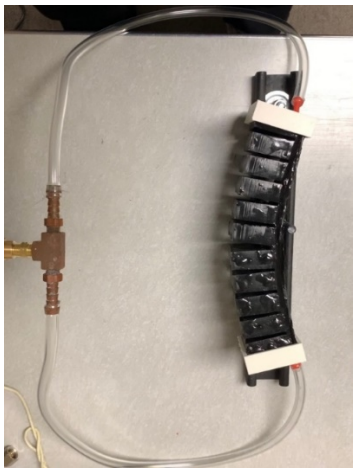

**Figure 10**: Knee actuator #1 unpressurized

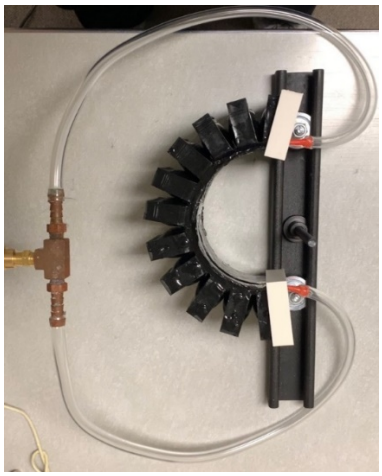

**Figure 11**: Knee actuator #1 pressurized

The second prototype has a slightly different design and it is shown in **Figure 13**. This model lacks the strain-limiting layer that causes bending. Instead, the wearer's knee will assume this function with the objective to increase the overall level of torque applied to the wearer's joints (43). In this case, the hollow chambers are connected by stretchable external tubing and an extendable layer, allowing elongation in the axial direction. Upon fluid pressurization, the chambers inflate and push against each other. Due to the extendable layer connecting the chambers, the actuator extends in the axial direction.

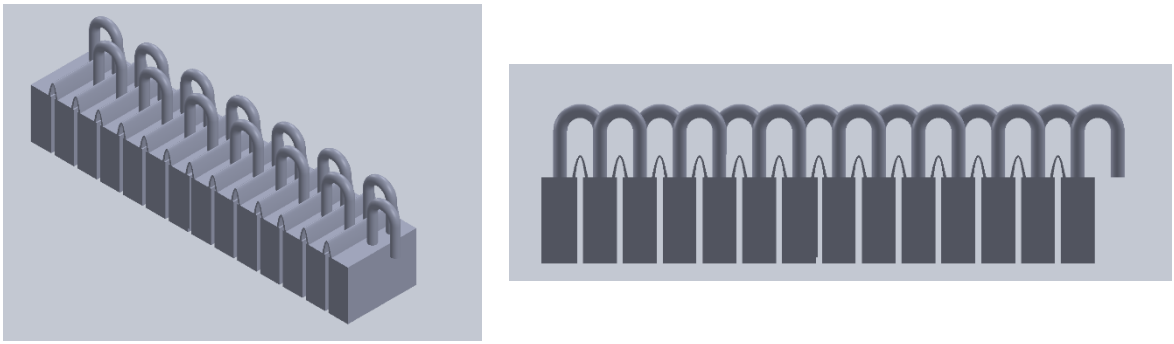

**Figure 12:** Knee soft-robotic actuator prototype #2 without integrated strain-limiting layer: isometric view (left) and front view (right). The chambers are connected to each other via external stretchable tubing and an extendable layer that allows elongation in the axial direction

### *3.1.2.2 Initial testing and Characterization*

To quantify the performance of the actuators, we implemented a 4-point bending test bed to characterize the relationship between pressure applied to actuate, torque produced, and angle generated. The theoretical framework is shown in **Figure 13**, where X indicates the region of interest of the beam to be tested, F is the force applied (to be chosen by the experimenter and applied symmetrically about the middle of the loading span), and D indicates the distance between the roller supports and the points where the forces are applied (D = 0.265 m for prototype #1 and D = 0.308 m for prototype #2). Thus, solving the associated free body diagram, the maximum torque generated by an actuator under a pre-defined force F is defined by: $M = \frac{1}{2}DF$.

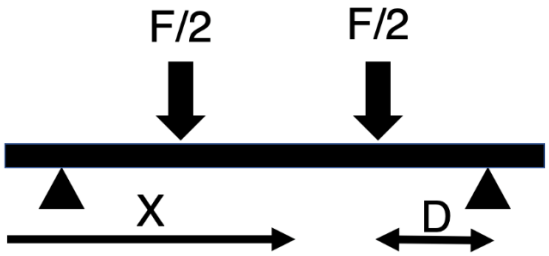


**Figure 13**: Theoretical framework for a four-point bending test bed, where X indicates the region of interest of the beam to be tested, F is the force applied and D indicates the distance between the roller supports and the points where the forces are applied

During testing, a known force was applied onto the actuator using two cables attached to known weights, and the actuator was pressurized at increasing increments. Additionally, blue markers were located on the actuator to calculate, at each pressure - force combination, the bending angle generated by the actuator (see **Figure 14**). A general view of the experimental setup is shown in **Figure 15**.

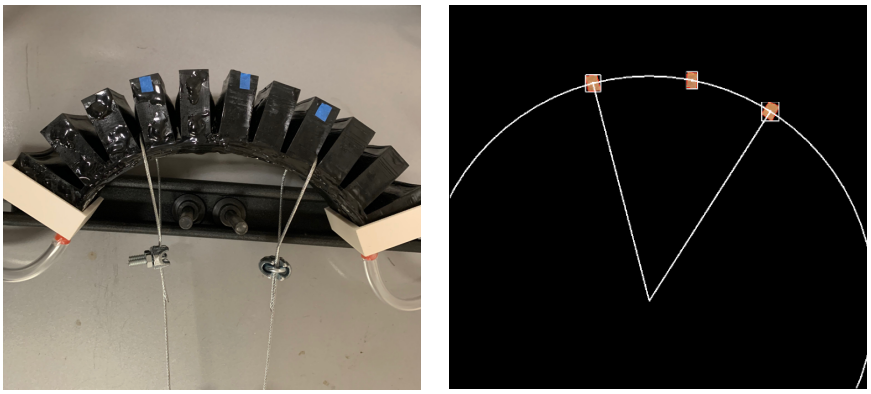

**Figure 14**: Actuator prototype #1 pressurized during four-point bending testing (left). The actuator has known forces applied and has three blue markers used to calculate the bending angle generated during pressurization at each pressure/force combination tested. The right image shows a screenshot of the script created to calculate the bending angle of the actuator based on the blue marker positions.

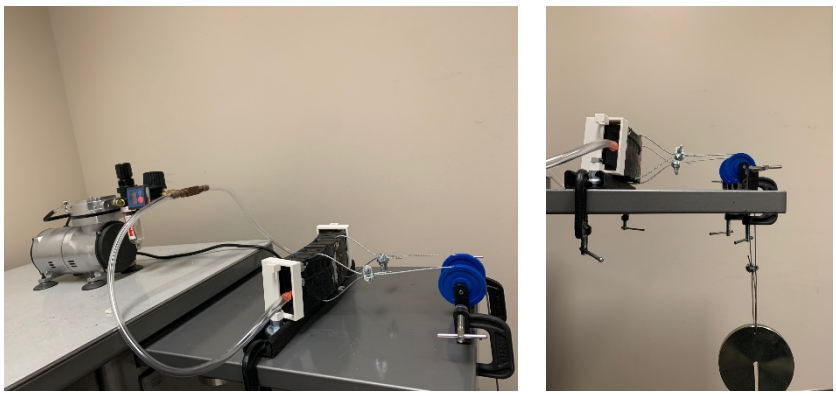

**Figure 15**: Four-point bending setup during testing of the actuator prototype #1. The actuator is connected to a pressurization source and a known force is applied via cables attached to known weights.

For prototype #1, testing pressures ranged from 1 to 15 psi, and the force load was increased in increments of 5 N, from 5 N to 35 N. Testing for a given force load was completed when the pressure reached 15 psi or the angle exceed 85 degrees, at which point the actuator would begin collapsing on itself. Results from actuator prototype #1 are shown in **Figure 16**.

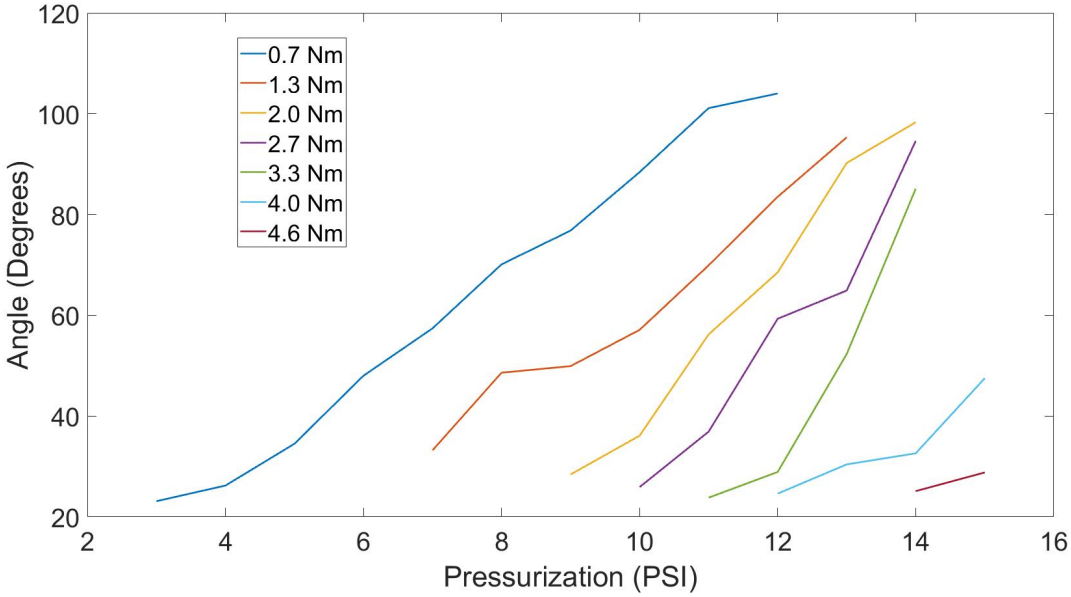


**Figure 16**: Relationship between pressure applied to actuate, torque produced, and bending angle generated by prototype #1. The higher the moment, the larger the pressure necessary to create the same angle. Alternatively, a larger torque for a given angle requires a higher pressure. The maximum torque generated by prototype #1 was ~4.6Nm at 15 psi.

Results showed that for a pressurization of 15 psi, our first prototype was already able to generate a torque of 4.6 Nm. The design of the actuator limited the angle at which the maximum torque can be achieved to approximately 24 degrees. For safety reasons, based on our relatively simple testing platform and since this was our first prototype, we decided not to go over 15 psi. Improved manufacturing and alternative feedstock would increase the safe levels of pressurization and the level of torque achieved.

For the prototype #2, we conducted a similar testing protocol using the same 4-point bending test bed (see **Figure 17**). Due to improved manufacturing, we were able to test up to 20 psi of pressure. The force load was increased in increments of 10N from 10N to 70N. Also, for testing purposes, we included an additional self-limiting layer (which was simulating the wearer's knee). Results, shown in **Figure 18**, indicated that **prototype #2 was capable of producing 10.7 Nm of torque at an angle of ~26 degrees when pressurized to 20 psi**.

Theoretically, we can calculate the expected assistive-net moment generated by the new actuator design. Using a pneumatic pressure differential, $\Delta p$= ~138 KPa (20 psi) and a knee radius (simulated with an artificial restrained layer) of r = 3 cm, the theoretical maximum soft-robotic induced moment yields $M_{N_{max}} = 11.7\ Nm$, which is very close to what we were able to achieve experimentally. This value is also higher than the maximum EMU induced knee torque during walking (~10 N m), and therefore enough to completely overcome the effort when bending the knee. Actuator performance and functional testing on an actual person still needs to be proven, including an investigation on how to better accommodate and fix the actuator onto the skin.

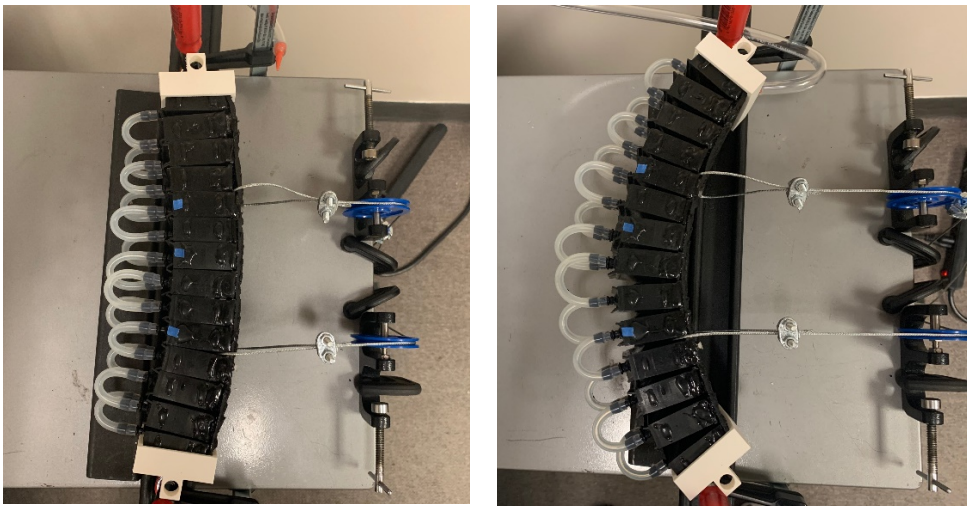

**Figure 17:** Prototype #2 depressurized (top left) and pressurized (top right) during 4-point bending testing.

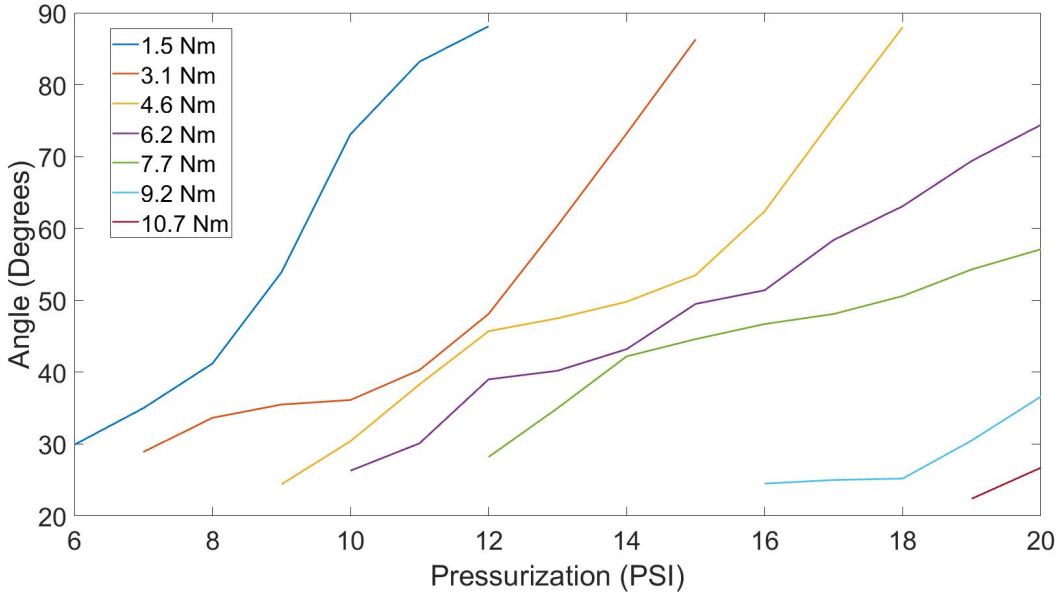


**Figure 18**: Relationship between pressure applied to actuate, torque produced, and bending angle generated by prototype #2. The higher the moment, the larger the pressure necessary to create the same angle. Alternatively, a larger torque for a given angle requires a higher pressure. The maximum torque generated by prototype #2 was ~10.7 Nm at 20psi.

### 3.1.3 Operational Impacts – Prebreathing Protocols

One key benefit of providing additional MCP is the reduction in pre-breathing times to avoid decompression sickness (DCS) before an EVA. DCS is an important consideration during EVA operations. To prevent DCS during exposure to spacesuit pressures (typically lower than the cabin pressure), astronauts prebreathe pure oxygen prior to depressurization to wash out nitrogen from body tissues. The duration of the prebreathing depends on the ambient atmosphere composition (cabin atmosphere in a trip to Mars) and the initial (i.e. cabin) and final (i.e. spacesuit) pressure.

The proposed soft-robotic layer, if extended over the entire body surface, has the potential to generate a continuous mechanical counterpressure. When strain limited, the elastomeric material comprising this layer can survive extreme pressures without rupture. Silicones, for example, have GPa bulk moduli. Therefore, when appropriately designed, an interior pneumatically pressurized elastomer lining can easily exceed 29.6 kPa inflation pressures. The key is to avoid unconstrained inflation that will lead to strains in excess of 100's %. The inflation of the lining can easily be directed towards the astronaut's skin, designing it to never expand beyond 100% strain and, therefore, never rupture.

In the context of the SmartSuit spacesuit, we investigated the relationships between the risk factor of decompression sickness (DCS), prebreathe time, and suit mobility with respect to the addition of mechanical counter pressure (MCP). MCP results from pressure applied to the skin from the soft-robotic elements integrated into the SmartSuit. To estimate the benefits of MCP from our soft robotic layers, we used prebreathing models that incorporate the evolution of nitrogen levels in human tissue while breathing pure oxygen to quantify the benefits of additional MCP on required prebreathing times and mobility.

A safety measure is the R-factor (19), also known as bends ratio, which is defined as:

$$R = \frac{P_{N2}}{P_{suit}}$$

where $P_{N2}$ is the initial absorbed tissue $N_2$ pressure (i.e. cabin $N_2$ partial pressure), and $P_{suit}$ is the spacesuit pressure. During pure oxygen prebreathe, the elimination of nitrogen follows an exponential decay curve with a tissue dependent half time, $t_{1/2}$ (typically equal to 360min), that can be expressed in terms of R value:

$$R(t) = R(0)\exp\left[-\ln(2)\frac{t}{t_{1/2}}\right]$$

Current NASA protocols are based on a final R value of ~1.65-1.7 after oxygen pre-breathe, and actual operational values are frequently between 1.3-1.4. Thus, for spacesuit pressures of 29.6 KPa (4.3 psi), a cabin standard atmosphere (101.3 KPa, 21% oxygen, 78% nitrogen) and a final R-value ~ 1.65-1.7, astronauts need to spend a total of 4 hours prebreathing pure oxygen (no exercise is assumed in our calculations).

**Figure 19** displays the relationship between suit pressure, prebreathe time, and DCS risk factor using a cabin pressure of standard atmospheric conditions (14.7 psi, 21% Oxygen, and 79% Nitrogen) like that found on the International Space Station (ISS). Similarly, **Figure 20** shows the same relationships under the conditions of the Space Shuttle before an EVA (10.3psi, 26.5% Oxygen, 73.5% Nitrogen).

**Figure 19** and **Figure 20** provide the expected results when compared to the protocol used on the ISS and Space Shuttle. Astronauts on ISS are exposed to atmospheres of 14.7 psi and 21% Oxygen as described above. During an EVA, the EMU spacesuit operates at 4.3psi (29.6 kPa) at 100% Oxygen, which requires a prebreathe time of 4 hours to achieve a risk factor of ~1.7 (actual operational values are frequently lower). Similarly, in the Shuttle (where the atmosphere could be manipulated to decrease prebreathing requirements before an EVA), astronauts conducted prebreathing during ~40min to achieve a risk factor of ~1.7.

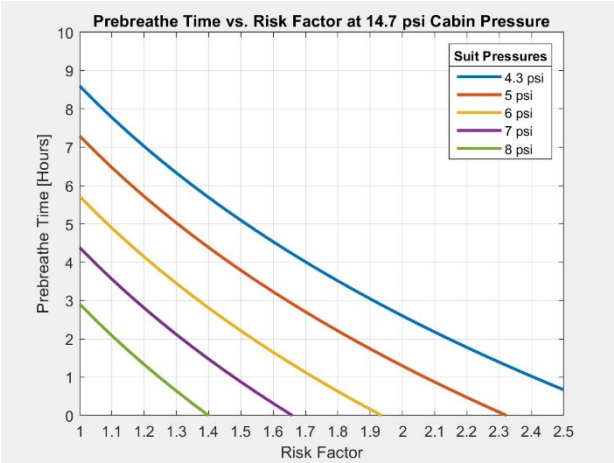


**Figure 19**: Relationship between spacesuit pressure, prebreathe times, and risk factor under ISS atmospheric cabin conditions (14.7 psi, 21% Oxygen, and 79% Nitrogen)

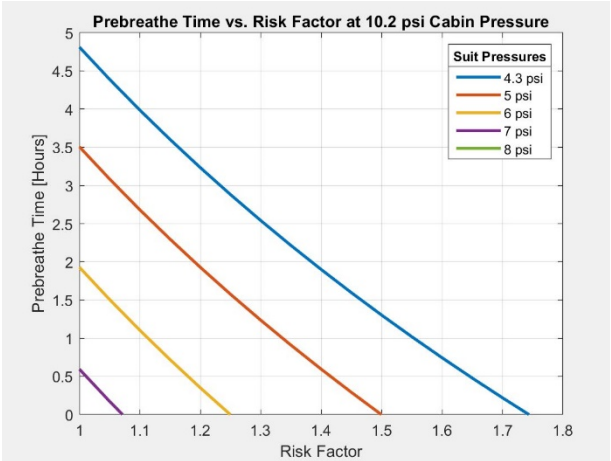


**Figure 20**: Relationship between spacesuit pressure, prebreathe times, and risk factor under Shuttle atmospheric cabin conditions (10.3psi, 26.5% Oxygen, 73.5% Nitrogen)

These figures show that, if the spacesuit pressure increases (due to the MCP from the soft-robotic layer), the prebreathe time required will decrease substantially. For example, in an ISS-like environment, if the soft-robotic layer can provide up to 10 kPa of additional pressure, the total pressure in the suit would be 29.6 + 10 = ~39.6 kPa ≈ 5.8 psi. Thus, for the same level of risk factor of R = 1.7, the **prebreathing times decreases from 4 hours to less than 2 hours**.

Operationally, once astronauts complete their pre-breathing protocol to achieve an initial operating pressure of ~39.6 kPa, the suit pressure can gradually step down to 29.6 kPa to conduct the majority of EVA tasks (following a similar concept of operations proposed for the Mark III). Since the soft-robotic layer already provides ~ 10KPa, the gas-generated pressure could be as low as ~20 kPa (or even lower if we achieve higher levels of MCP), further enhancing mobility, facilitating even more joint movements and thus surface exploration.

In an attempt to quantify mobility in the present context, we use "Difficulty of Movement" (DM), defined by Huerta (17) as a quantity that describes how easy or how hard it is to perform movements. It ranges from 0 (least difficult) to 1 (most difficult). Elevated gas pressurization will highly decrease mobility. MCP suits will also decrease mobility, but to a much lesser extent. The following equations described by Huerta (17) quantify the Difficulty of Movement (DM) in both a gas pressurized spacesuit and a MCP spacesuit:

$$DM_{Gas\ Pressurized} = \frac{\frac{1}{14.7}P_{gas} + 0.125}{1.125}$$

$$DM_{MCP} = (0.27 - 0.05)/1.125$$

$DM_{Gas\ Pressurized}$ increases as gas pressure increases while $DM_{MCP}$ stays constant at a relatively low level, meaning that mobility is not affected by changes in MCP levels.

**Figure 21** shows the relationship between suit pressure and difficulty of movement (DM) as a function of the percentage of MCP applied (with respect to the total pressure of the suit). A linear relationship has been assumed between the $DM_{Gas\ Pressurized}$ when the spacesuit in 100% gas pressurized (0% MCP contribution) and the case where the spacesuit is pressurized with only MCP $DM_{MCP}$ (100% MCP contribution). If MCP increases, (replacing some of the gas pressure), spacesuit joint torques will be reduced and thus, overall mobility will improve. According to **Figure 21**, in a 4.3 psi gas-pressurized spacesuit, 1 psi of MCP will improve mobility by ~11%. Finally, **Figure 22** shows the relationship between % MCP (with respect to the total pressure of the suit), difficulty of movement and prebreathe time.

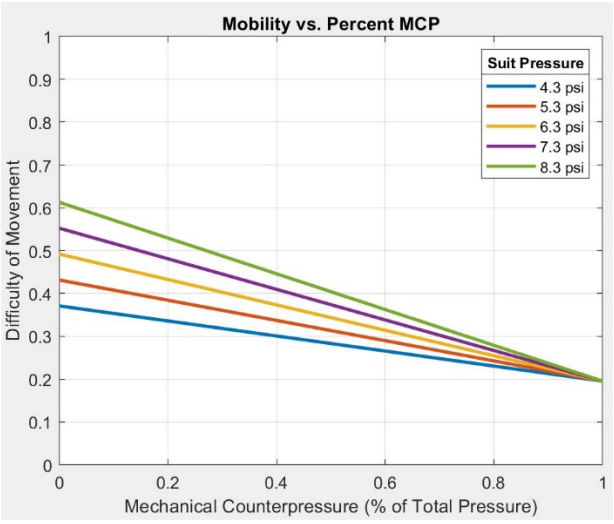


**Figure 21**: Relationship between suit pressure, mobility, and % MCP (from 0-no MCP to 1-all MCP) under ISS atmospheric cabin conditions (14.7 psi, 21% Oxygen, and 79% Nitrogen)

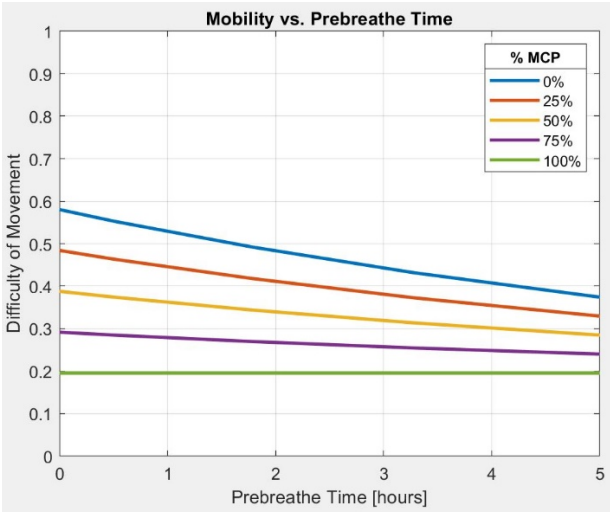


**Figure 22:** Relationship between suit pressure, mobility, and prebreathe times under ISS atmospheric cabin conditions (14.7 psi, 21% Oxygen, and 79% Nitrogen)

Finally, to view and understand these tradeoffs more easily, as well as explain these concepts in a more graphical way in a classroom setting, we have developed a computational tool that is capable of generating these relationships automatically. Variable parameters include cabin conditions, total suit pressure, gas pressure, mechanical counterpressure, decompression sickness risk factor, prebreathing times, and difficulty of movement. A screenshot of the GUI is shown in **Figure 23**.

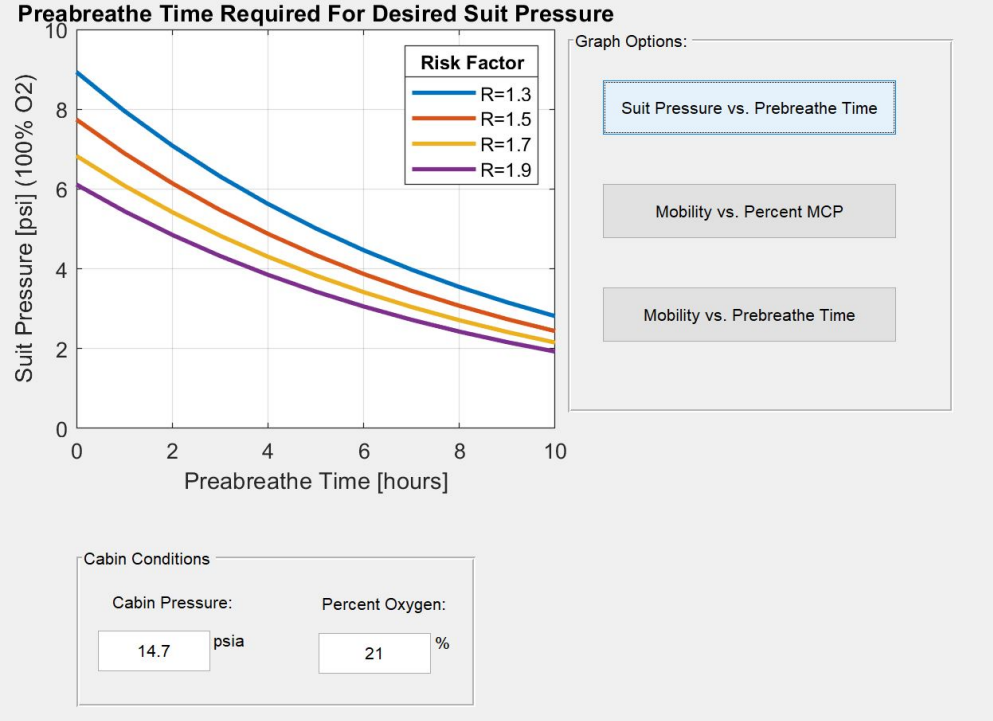


**Figure 23:** GUI of the computational tool developed. Parameters of interested include cabin conditions, total suit pressure, gas pressure, mechanical counterpressure, decompression sickness risk factor, prebreathing times, and difficulty of movement

## 3.2 Self-Healing Sensory Membrane with Embedded OptoElectronic Sensing

In recent years, stretchable sensors for wearable applications have demonstrated their capabilities of continuous health monitoring with high levels of fidelity and comfort. Integrating these stretchable sensors into spacesuits could provide valuable insights into astronauts' movements during EVA. Co-I Shepherd has developed a new class of stretchable sensors based on optical waveguides, which has shown to have high sensitivity, accuracy, repeatability, and low hysteresis.

Using elastomeric material (i.e., silicones and polyurethanes), Co-I Shepherd has created lightguides that change power output upon stretching (**Figure 24**), we call these sensors Lightlace™ (submitted for trademark to USPTO). Light exits the lightguide by exceeding the critical angle for total internal reflection upon localized deformation. The degree of light loss is logarithmically proportional to the amount of linear strain (**Figure 24**E).

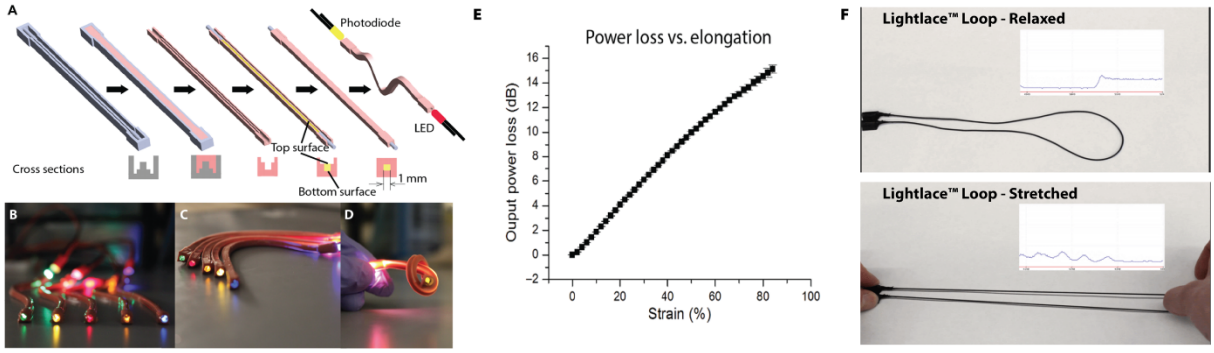


**Figure 24:** (**A-E**) Initial fabrication route for soft, stretchable optical lightguides that decrease in power output upon stretching. (**F**) Commercialized Lightlace™ Loop that we fabricate in two meter lengths, 20 at a time for soft strain sensor. The electronics are contained on the left side and light is pumped through a loop on the right side. Allowing the sensor to be totally soft, tough, and moisture resistant in the area of use.

A matrix of Lightlace™ consists of nodes of intersecting powered and unpowered stretchable optical lightguides in 2D and 3D arrays (see **Figure 25**) (41). When these lightguides contact, light is coupled between them proportional to amount of stress and strain applied. These networks, therefore, provide localization of multiple deformation positions, as well as the amplitude of deformation. We have shown that these arrays can be threaded into a foam matrix for location and pressure information of external touch (**Figure 25** C,D).

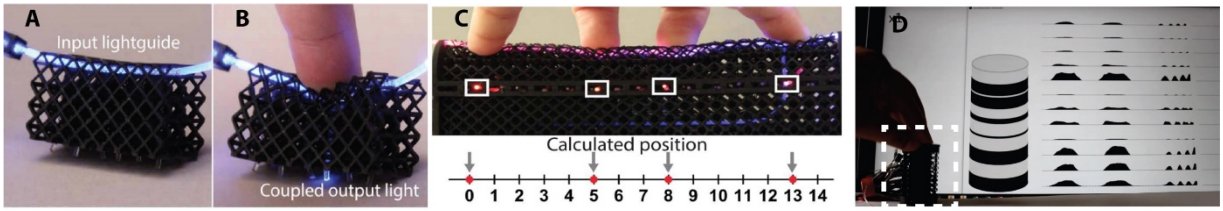


**Figure 25:** (**A,B**) Contact from multiple lightguides leads to coupling via Frustrated Total Internal Reflection. (**C**) Using the coupled light node location and intensity, the location and magnitude of touch pressure can be reconstructed at multiple locations. (**D**) A cylindrical network of Lightlace™ (dashed white box) can reconstruct the shape of the cylinder under load. Raw output from lightguides is shown next to virtual cylinder shape reconstruction.

Lightlace™ has recently been stitched onto garments for use in measuring human performance. **Figure 27** left shows an array of laser diodes illuminating three separate stretchable lightguides as a conceptual prototype. **Figure 27**,middle,right shows a functional prototype with reconstructed joint angle.

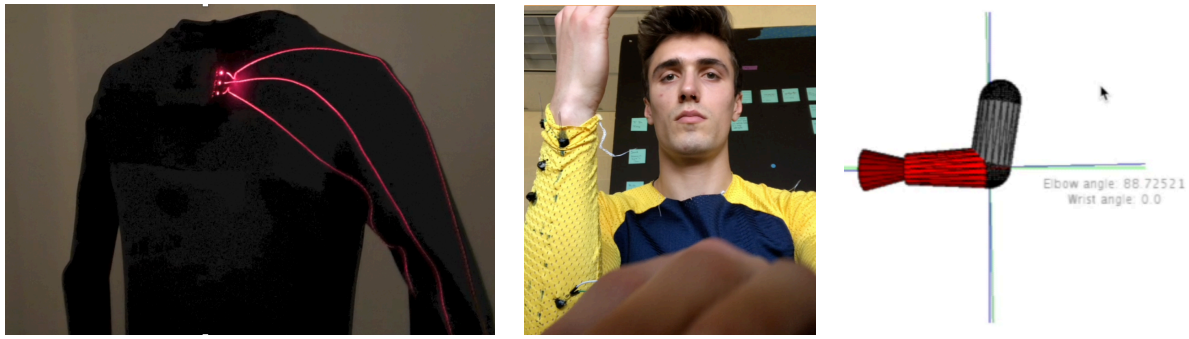


**Figure 26:** LightLace™ is a wearable sensor suite capable of measuring pressure and motion across the whole body.

Our efforts in Lightlace™ have been supported previously as research grants within the Organic Robotics Laboratory at Cornell University. It has been supported by three separate research grants from the DoD (2 AFOSR and 1 ONR), as well as an NSF EAGER. This EAGER was supported under grant #CMMI 1745139, DCSD: Eager: Reliable Control for Soft Robots Through Sensor Placement. These works have resulted in four provisional patent applications specific to Lightlace™, and several more being drafted, the first of which was submitted in early 2016. The efforts also resulted in several high impact, peer-reviewed publications (15, 24, 41–44).

Safety is the most important factor when it comes to spacesuit design. The ability to monitor the integrity of the spacesuit in case of adverse events, such as falling or puncture, is essential. Furthermore, the capability for the spacesuit to self-heal from those adverse events is desirable. To satisfy these needs, we propose a stretchable sensory membrane that not only monitors the astronauts' movements but, as importantly, senses damage and self-heals from them. Our approach is to develop a self-healing material that can also be used as a stretchable optical waveguide sensor.

### 3.2.1 Requirements for the self-healing material as optical sensor

We first characterized how a stretchable optical sensor behaves under damage without self-healing ability. **Figure 27** shows the response of cutting a non-self-healable transparent polyurethane waveguide embedded in a silicone matrix. From the change of the output intensity we can see 1) the sensor is able to sense damage (cuts) as measured output intensity decreases towards zero; 2) after the cut, the sensor can resume to sense deformations (presses); 3) after each cut, the level of undeformed intensity is attenuated. With several control experiments, we have found the major reasons for the intensity attenuation is from the crack introduced by the cut, and misalignment of the waveguide at the cut. For the optical sensor to self-heal from the damage (i.e. resume pristine intensity level), the former observation poses the requirement for the self-healing material to be able to heal the crack, and the latter requires this material to be tough and resilient.

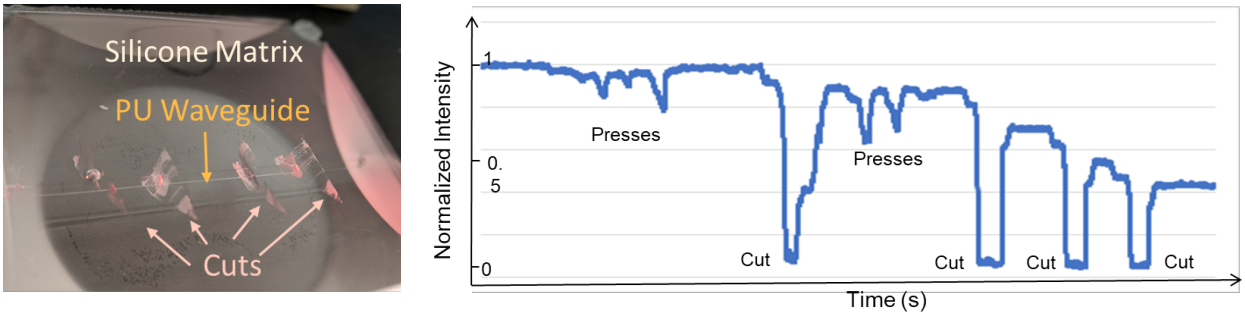


**Figure 27:** Pressing and cutting non self-healable waveguide sensor.

### 3.2.2 Self-healing material

Self-healing materials can be characterized into extrinsic self-healing and intrinsic self-healing. Extrinsic self-healing materials usually involves encapsulated microdroplets that can initiate polymerization once punctured. This approach is limited in the number of times it can heal. Therefore, we choose to make an intrinsic self-healing material, which can be cut and healed infinite times due to the mechanisms of the dynamic bonds.

During Phase I, we designed a self-healing material based on polyurethane urea elastomer (sPUU), with soft segments composed of polytetramethylene glycol (PTMEG, Mw=1,000) and isophorone diisocyanate (IPDI), and a hard segment of bis(4-hydroxyphenyl) disulfide (disulfide bridge, or S-S; see **Figure 29**). Self-healing is enabled mainly by the strong dynamic covalent bond of the disulfide bridge (bond energy 251 kJ/mol), and partially assisted by the hydrogen bond from the urea groups (bond energy 8 kJ/mol). This is an intrinsic self-healing material, meaning that it can, theoretically, be cut and healed infinite times due to the mechanisms of the dynamic bonds. The aromatic disulfide bond adopted belongs to the family of associative covalent networks (CAN), where the cleavage and formation of bonds are concerted. Compared to dissociative CANs like Diels-Alder chemistry, where new bonds could only form after existing bonds are broken and thus requires controlled heating, the aromatic disulfide bond enables our sPUU to self-heal in room temperature, without any need for heat, light, or catalyst. Furthermore, thanks to the strong disulfide bond, the sPUU also has the desirable mechanical property of high toughness.

### 3.2.3 Self-healing Properties

To characterize the self-healing properties of the sPUU, we first observed the cracks self-healing in room temperature both in macroscopic and microscopic scale (see **Figure 29**). In the macroscopic case we made a 1 cm long, 2 mm deep cut on the surface of the material. The crack completely self-heals in room temperature in 12 hours. In the microscopic case, we made a scratch on the material, and observed through a microscope. We found that the scratch has mostly self-healed in room temperature in one hour. These experiments show that the crack introduced by a cut could quickly self-heal under room temperature, satisfying the aforementioned material requirement.

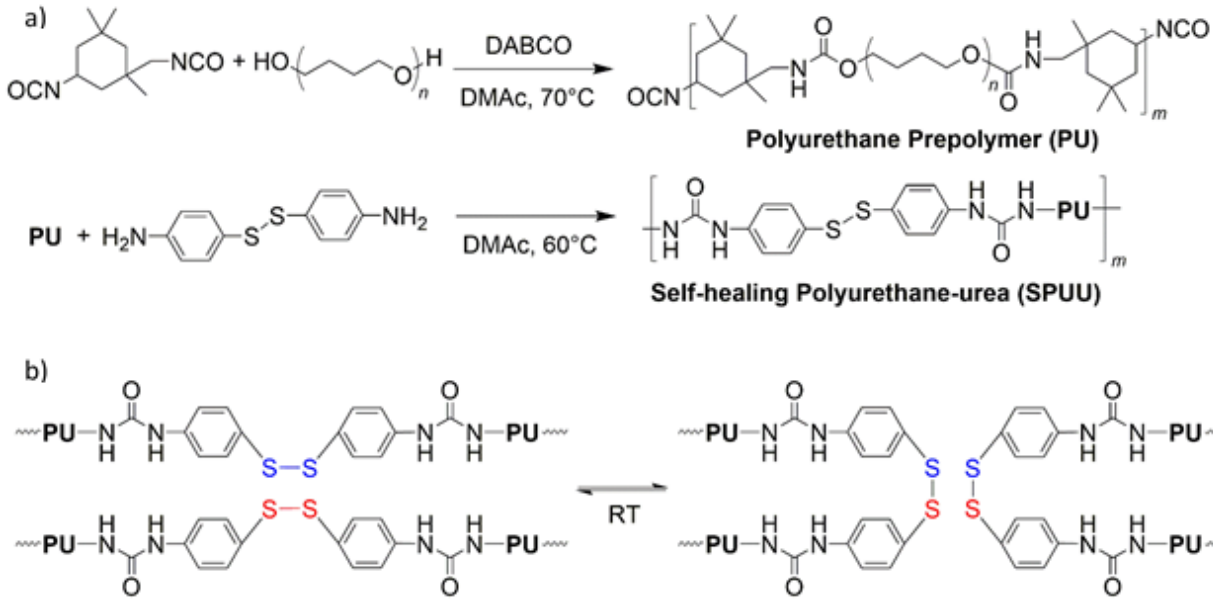


**Figure 28:** a) schematic and synthesis of the sPUU; b) self-healing mechanism via disulfide metathesis.

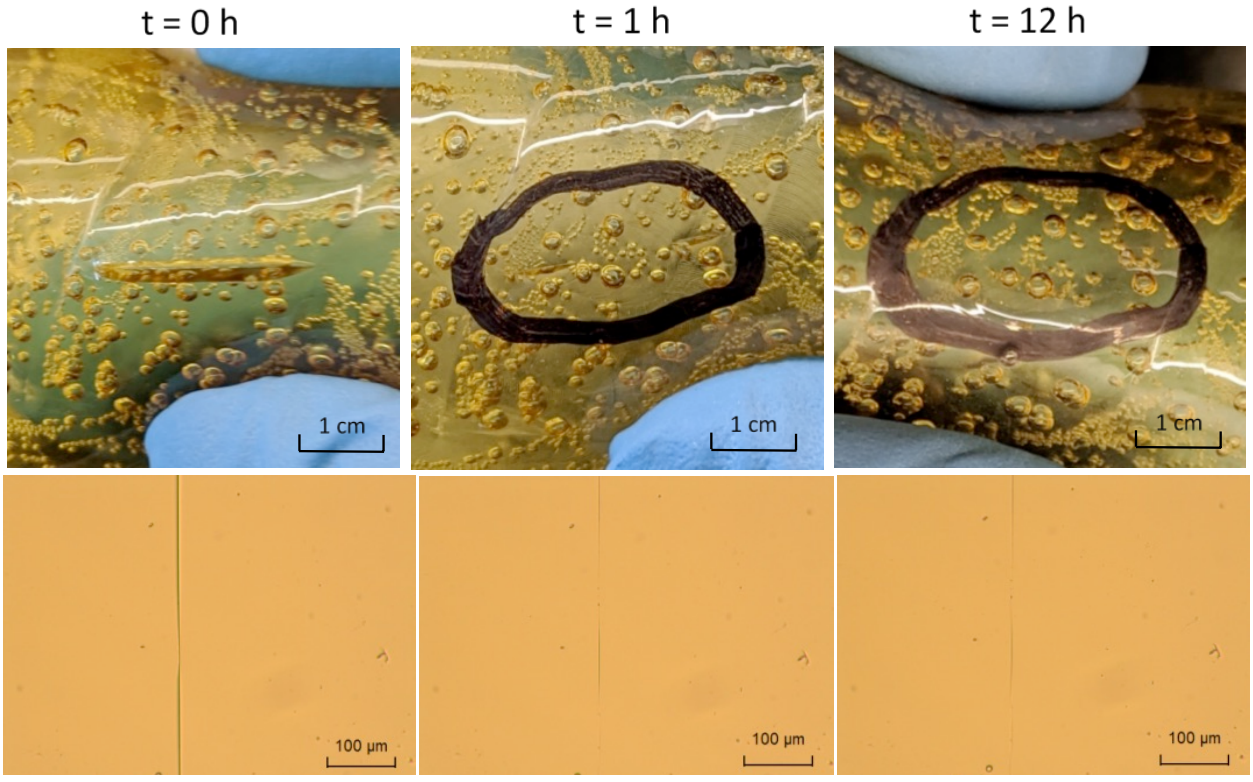


**Figure 29:** Macroscopic and microscopic pictures of cracks self-healing in room temperature at 1h and 12h : a) 2 mm deep crack self-heals in room temperature; b) microscopic image of a scratch self-healing in room temperature

Additionally, we also conducted tensile tests to further characterize sPUU's self-healing properties of mechanical strength (see **Figure 30**). The pristine sample exhibited good mechanical properties of high stretchability and high toughness (ultimate strain ~ 14, ultimate stress ~ 4.5 MPa). Samples were cut and self-healed in room temperature for 1 hour, 6 hours, and 24 hours. Results in **Figure 30** showed that sPUU's self-healing efficiency is 52% at 1 hour, 65% at 6 hours, and 77% at 24 hours at room temperature in terms of stretchability. All samples stretch nearly identically up to 700% strain, far in excess of any expected strain an astronaut would encounter interacting with their environment during EVA.

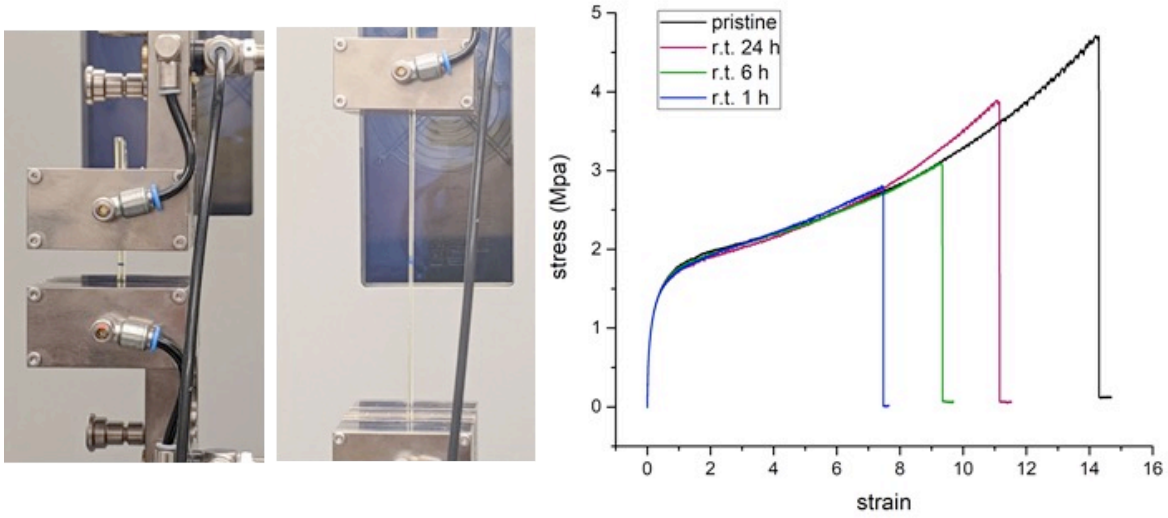


**Figure 30:** Tensile test to characterize sPPU's self-healing efficiency at room temperature.

Finally, we characterized light propagation conditions in our sPUU material, which is an important requirement for use as an optical lightguide sensor. Testing results showed that this sPUU has excellent transparency (~90% with 1 mm thick sample) in red and near infrared wavelength (**Figure 31** left). **Figure 31** right shows a waveguide made of sPUU transmitting red light from a LED.

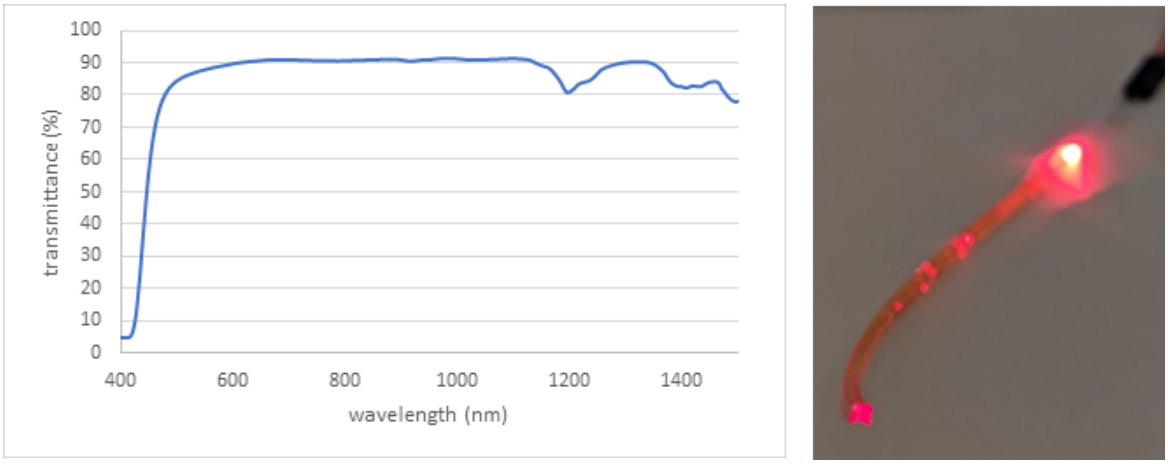


**Figure 31**: Transmittance of sPUU measured by UV-Vis (left); sPUU waveguide transmitting light (right).

### 3.2.4 Self-healing material as optical waveguide sensor

Our sPUU material satisfies the self-healing, optical, and mechanical properties concluded previously; therefore, we made an optical waveguide sensor with sPUU embedded in a matrix of PDMS. We fitted a red LED on one end and a photodiode on the other end (see **Figure 32**). By detecting the intensity change at the output, we can know when the sensor is deformed and damaged. Enabled by the sPUU, the sensor is able to self-heal and recover to its original signal level after damage.

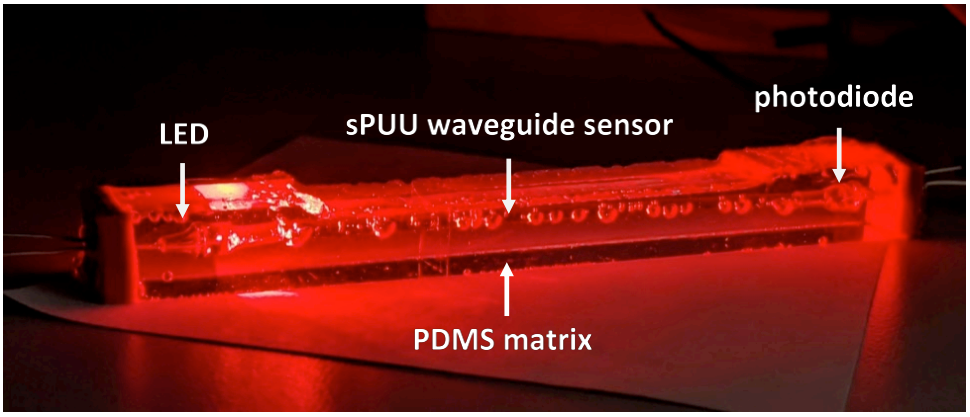


**Figure 32:** Photo of self-healing optical waveguide sensor embedded in PDMS matrix

**Figure 33** shows the self-healing sensors' responses before, during, and after the damage of a cut. At the onset of a cut by a razor blade, the normalized intensity decreases from 1 to 0, indicating damage to the membrane. When the blade is taken away, the assembly at the cut location is lifted with the two damaged sensor faces partially touching as indicated by the partially recovered signal. By manually pushing the assembly back down on the table, the two cut faces touch and align again. The intensity signal fully recovers once the faces are aligned. It is likely that a spacesuit with these sensors would self-heal without intervention from the astronaut; however, the astronaut could also aid in healing by pressing the ruptured components together. In the case of external pressure provided by the astronaut, it is likely the speed of healing would rapidly increase. This hypothesis will be tested in Phase 2.

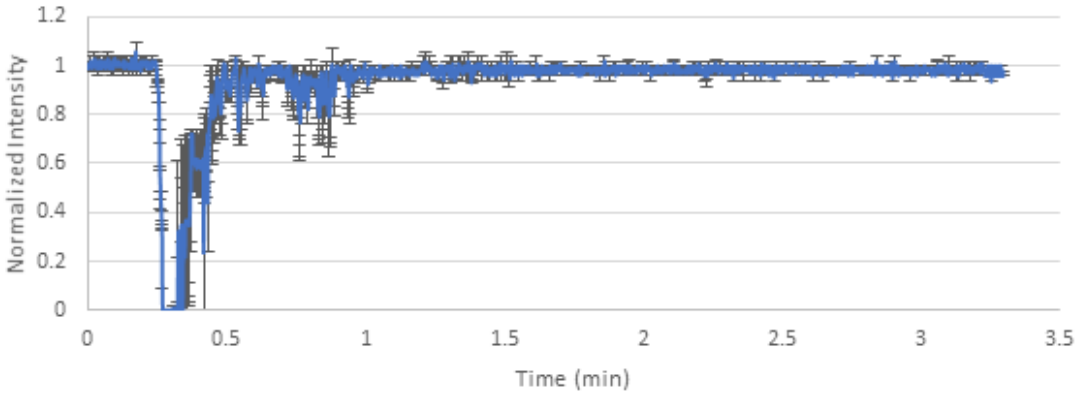


**Figure 33:** Waveguide sensor intensity fully recovers after a cut (3 sets of data, blue line indicates average)

*sPUU material temperature characterization*

EVA on Mars might occur under extreme temperature changes. Thus, we have also characterized sPUU's working range of temperatures. Differential scanning calorimetry (DSC) test showed that glass transition temperature for sPUU is -42.12°C, where this elastomer transitions to glassy state below this temperature. Thermogravimetric analysis (TGA) shows sPUU starts to decompose at 331.29°C. Temperature on Mars changes between +20°C to -125°C. The sPUU working range of temperature suggests that the self-healing sensing layer in the current state might need to be protected by other temperature insulating layers or active heating methods, or else EVA's could be limited to daylight hours and warmer latitudes.

# 4 Overall Benefit in Future Mission Scenarios

## 4.1 Design Reference Mission 5.0

In the context of the Mars Design Reference Architecture 5.0 (9) (8), a standard mission to Mars would result in approximately 18 months on the surface of the planet, which is equivalent to up to 540 days for planetary EVAs [18]. Assuming an average of four weekly EVAs, each crew member would accomplish ~300 EVAs per Martian stay. Expected "traversing distances" for these EVAs are estimated at 1-2km before a pressurized or unpressurized rover would be used (4). Then, we could assume that in each EVA, crewmembers walk at least 2 km to get to/from the target EVA site plus some additional walking on the actual site, which we estimate about an additional hour walking. Assuming a gait cycle (GC) that last 1.1 second and traverses 1.4 m, we can estimate the total walking time during an EVA to be approximately 1.44 hours (equivalent to 1hour 26 min; 2000m * 1.1sec/GC * (1/1.4 m/GC) = 26 min plus 1 additional hour walking on site). Based on the metabolic energy expenditure shown in Table 1, **the Smartsuit would save one crew member ~ 50,000 kilocalories on a 18-month expedition to Mars** ((957-842) Kcal/hour * 1.44 hours/EVA * 300 EVAs = 49680 Kcal). Additionally, the reduction in EVA preparation time combined with the increase in safety (due to the self-healing membrane), and the enhanced interaction with the environment (due to the optoelectronic sensors) will increase the overall human performance by orders of magnitude.

# 5 Earth Benefits and Alternate Uses

If the concept eventually succeeds, it will enable a new approach to develop EVA suits for performing planetary surface EVA, notably on Mars. Our concept will enhance human mobility, both on space and Earth applications, but the same soft-robotics principles could be applicable to surface robotics applications. More broadly, the co-integration of optoelectronic sensing and visualization into self-healing membranes will provide a new smart material platform for space exploration. Other potential applications include large-scale habitats or landing airbags, where structural health becomes a priority.

Beyond the space applications, extending the applicability of this exotic concept to terrestrial applications is in the best traditions of NASA's spinoffs and offers additional economic benefit. The proposed spacesuit, or single-person spacecraft architecture could be applicable to other on-Earth activities such as deep see diving, where bulky and gas-pressurized suits are also used. Additionally, the application of this unique spacecraft technology development extends to other terrestrial applications such as coatings to vehicles and buildings for structural health monitoring and safety monitors, or integration into clothing as a wearable technology for sports/fitness applications or for soldier performance, health, camouflage, and signaling.

# 6 Outreach and Broader Impacts

During Phase I of this project, our team has been very proactive at engaging with the community and the general public. PI Diaz Artiles and the rest of the team has participated in multiple conferences and seminars nationally and internationally, to talk about our SmartSuit concept and the technologies being developed. Additionally, we will participate in the "2020 Science Fiction to Science Fact" event to be held next April at the Chicago Museum of Science and Industry, where we will have the opportunity to bring our science and technology closer to middle school and high school students. We are also currently working on several publications, including one for the 50$^{th}$ International Conference of Environmental Systems to present results from our study to the spacesuit community.

# 7 References

1. **Anderson A**, **Diaz A**, **Kracik M**, **Trotti G**, **Hoffman J**, **Newman D**. Developing a Spacesuit Injury Countermeasure System for Extravehicular Activity: Modeling and Analysis. *42nd Int Conf Environ Syst* : 1–10, 2012.

2. **Anderson AP**, **Diaz A**, **Kracik M**, **Trotti G**, **Hoffman J**, **Newman DJ**. Understanding Human-spacesuit Interaction to Prevent Injury during Extravehicular Activity. In: *NASA Human Research Program Investigator's Workshop*. Houston, TX: 2013.

3. **Anderson FC**, **Pandy MG**. A Dynamic Optimization Solution for Vertical Jumping in Three Dimensions. *Comput Methods Biomech Biomed Engin* 2: 201–231, 1999.

4. **Anderson FC**, **Pandy MG**. Dynamic Optimization of Human Walking. *J Biomech Eng* 123: 381, 2001.

5. **Beaucage-Gauvreau E**, **Robertson WSP**, **Brandon SCE**, **Fraser R**, **Freeman BJC**, **Graham RB**, **Thewlis D**, **Jones CF**. Validation of an OpenSim full-body model with detailed lumbar spine for estimating lower lumbar spine loads during symmetric and asymmetric lifting tasks. *Comput Methods Biomech Biomed Engin* 22, 2019.

6. **Carr CE**, **Newman DJ**. Space Suit Bioenergetics : Cost of Transport During Walking and Running. *Aviat Space Environ Med* 78: 1093–1102, 2007.

7. **Carr CE**, **Newman DJ**. Space Suit Bioenergetics : Framework and Analysis of Unsuited and Suited Activity. *Aviat Space Environ Med* 78: 1013–1022, 2007.

8. **Delp SL**, **Anderson FC**, **Arnold AS**, **Loan P**, **Habib A**, **John CT**, **Guendelman E**, **Thelen DG**. OpenSim: open-source software to create and analyze dynamic simulations of movement. *IEEE Trans Biomed Eng* 54: 1940–50, 2007.

9. **Diaz A**. Musculoskeletal Human-Spacesuit Interaction Model. *IEEE Aerosp Conf Proc* 2014-June, 2014.

10. **Diaz A**, **Anderson A**, **Kracik M**, **Trotti G**, **Hoffman J**. Development of a Comprehensive Astronaut Spacesuit Injury Database. In: *63rd International Astronautical Congress*. Naples, Italy: 2012, p. 1–9.

11. **Diaz A**, **Anderson AP**, **Kracik M**, **Trotti G**, **Newman DJ**. Development of a musculoskeletal human spacesuit interaction model. In: *NASA Human Research Program Investigator's Workshop*. Houston, TX: 2013.

12. **Gilkey AL**. Space Suit Simulator for Partial Gravity Extravehicular Activity Experimentation and Training. Massachusetts Institute of Technology: 2012.

13. **Goel R**, **Kaderka J**, **Newman D**. Modeling the benefits of an artificial gravity countermeasure coupled with exercise and vibration. *Acta Astronaut* 70: 43–51, 2012.

14. **Hamner SR**, **Seth A**, **Delp SL**. Muscle contributions to propulsion and support during running. *J Biomech* 43: 2709–16, 2010.

15. **Harnett CK**, **Zhao H**, **Shepherd RF**. Stretchable Optical Fibers: Threads for Strain-

Sensitive Textiles. *Adv Mater Technol* 2, 2017.

16. **Hilbert A**, **Diaz A**, **Anderson AP**, **Newman DJ**. Human Spacesuit Interaction: Musculoskeletal Modeling and Statistical Analysis of Injuries. In: *NASA Human Research Program Investigator's Workshop*. Galveston, TX: 2014.

17. **Huerta R**, **Kerr ES**, **Anderson AP**, **Sickness D**, **Activity E**, **Pressurized G**, **Counterpressure M**, **Meter N**, **Pressure F**, **Pressure GA**, **Joint PI**, **Life P**, **Systems S**, **Pressure PN**, **Inch PS**, **Student M**, **Student U**. Spacesuit Concept to Enable Martian Planetary Exploration. In: *48th International Conference of Environmental Systems*. Albuquerque, New Mexico: 2018.

18. **John CT**. Residual Reduction Algorithm ( RRA ). 2008.

19. **Lange KE**, **Perka AT**, **Duffield BE**, **Jeng FF**. Bounding the Spacecraft Atmosphere Design Space for Future Exploration Missions. *Nasa/Cr—2005–213689* : 213689, 2005.

20. **Newman DJ**. Life Support and Performance Issues for Extravehicular Activity. In: *Fundamentals of Life Sciences*. 1997.

21. **Newman DJ**, **Anderson A**, **Diaz A**, **Kracik M**, **Hilbert A**, **Bertrand P**, **Hoffman J**, **Trotti G**. Spacesuit Trauma Countermeasures Research: Injury Prevention and Comfort Protection Design. In: *2014 NASA Human Research Program Investigators' Workshop*. Galveston, TX: 2014.

22. **Newman DJ**, **Anderson AP**, **Bertrand P**, **Diaz A**, **Hilbert A**, **Hoffman J**, **Kracik M**, **Reyes S**, **Trotti G**. Conclusions and Paths Forward in Space Suit Injury Countermeasures. In: *2015 NASA Human Research Program Investigator's Workshop*. Galveston, TX: 2015.

23. **Norcross JR**, **Clowers KG**, **Clark T**, **Harvill L**, **Morency RM**. *Metabolic Costs and Biomechanics of Level Ambulation in a Planetary Suit*. National Aeronautics and Space Administration, February, 2010.

24. **O'Brien KW**, **Xu PA**, **Levine DJ**, **Aubin CA**, **Yang HJ**, **Xiao MF**, **Wiesner LW**, **Shepherd RF**. Elastomeric passive transmission for autonomous force-velocity adaptation applied to 3D-printed prosthetics. *Sci Robot* 3, 2018.

25. **Opperman RA**, **Waldie JMA**, **Natapoff A**, **Newman DJ**, **Jones JA**. Probability of Spacesuit-Induced Fingernail Trauma Is Associated with Hand Circumference. *Aviat Space Environ Med* 81: 907–913, 2010.

26. **Raabe ME**, **Chaudhari AMW**. An investigation of jogging biomechanics using the full-body lumbar spine model: Model development and validation. *J Biomech* 49: 1238–1243, 2016.

27. **Rückert EA**, **Neumann G**. Stochastic optimal control methods for investigating the power of morphological computation. *Artif Life* 19: 115–131, 2013.

28. **Scheuring RA**, **Mathers CH**, **Jones JA**, **Wear ML**. Musculoskeletal Injuries and Minor Trauma in Space: Incidence and Injury Mechanisms in U.S. Astronauts. *Aviat Space Environ Med* 80: 117–124, 2009.

29. **Schmidt PB**, **Newman DJ**, **Hodgson E**. Modeling Space Suit Mobility: Applications to Design and Operations. In: *31st International Conference on Environmental Systems*.

30. **Shen Z**, **Sam S**, **Allison G**, **Cui L**. A simulation-based study on a clutch-spring mechanism reducing human walking metabolic cost. *Int J Mech Eng Robot Res* 7: 55–60, 2018.

31. **Silder A**, **Besier T**, **Delp SL**. Predicting the metabolic cost of incline walking from muscle activity and walking mechanics. *J Biomech* 45: 1842–9, 2012.

32. **Strauss S**. Extravehicular Mobility Unit Training Suit Symptom Study Report. 2004.

33. **Strauss S**, **Krog RL**, **Feiveson AH**. Extravehicular mobility unit training and astronaut injuries. [Online]. *Aviat Space Environ Med* 76: 469–74, 2005. http://www.ncbi.nlm.nih.gov/pubmed/15892545.

34. **Thelen DG**, **Anderson FC**. Using computed muscle control to generate forward dynamic simulations of human walking from experimental data. *J Biomech* 39: 1107–15, 2006.

35. **Thelen DG**, **Anderson FC**, **Delp SL**. Generating dynamic simulations of movement using computed muscle control. *J Biomech* 36: 321–328, 2003.

36. **Thomas KS**, **McMann HJ**. *U. S. Spacesuits*. Second Edi. Springer Science & Business Media, 2012.

37. **Trivedi D**, **Rahn CD**, **Kier WM**, **Walker ID**. Soft robotics: Biological inspiration, state of the art, and future research. *Appl Bionics Biomech* 5: 99–117, 2008.

38. **Umberger BR**. Stance and swing phase costs in human walking. *J R Soc Interface* 7: 1329–1340, 2010.

39. **Umberger BR**, **Gerritsen KGM**, **Martin PE**. A model of human muscle energy expenditure. *Comput Methods Biomech Biomed Engin* 6: 99–111, 2003.

40. **Williams DR**, **Johnson BJ**. EMU Shoulder Injury Tiger Team Report. 2003.

41. **Xu PA**, **Mishra AK**, **Bai H**, **Aubin CA**, **Zullo L**, **Shepherd RF**. Optical lace for synthetic afferent neural networks. *Sci Robot* in press, 2019.

42. **Zhao H**, **Huang R**, **Shepherd RF**. Curvature control of soft orthotics via low cost solid-state optics. In: *Proceedings - IEEE International Conference on Robotics and Automation*. 2016, p. 4008–4013.

43. **Zhao H**, **Jalving J**, **Huang R**, **Knepper R**, **Ruina A**, **Shepherd R**. A helping hand: Soft orthosis with integrated optical strain sensors and EMG control. *IEEE Robot Autom Mag* 23: 55–64, 2016.

44. **Zhao H**, **O'Brien K**, **Li S**, **Shepherd R**. Optoelectronically Innervated Soft Prosthetic Hand via Stretchable Optical Waveguides. *Sci Robot* 1: 7529, 2016.

# 8 Appendices

## 8.1 Invited Talks, Publications, and Outreach

1. A. Diaz Artiles, "SmartSuit for Extravehicular Activity: Current Challenges and Spacesuit Technology Development to Enable Future Planetary Exploration Missions". *LIFE2019 Landmark Innovation Forum & Expo – Imagine! Track*, Houston, TX, August 28, 2019.
2. A. Diaz-Artiles. R. Shepherd, L. Kluis, N. Keller, H. Bai, N. Iyengar, Chase Audirsch "SmartSuit: A Hybrid, Intelligent, and Highly Mobile EVA Spacesuit for Next Generation Exploration Missions" (presentation + poster). *2019 NASA Innovative Advanced Concepts (NIAC) Symposium*, Huntsville, AL, September 24-26, 2019.
3. A. Diaz Artiles and J. Gomez-Elvira (invited technical talk). "Una Perspectiva de la Exploración Humana y Robótica del Espacio". *Universidad de Nebrija*, Madrid, Spain, November 7, 2019.
4. L. Kluis, N. Keller, H. Bai, N. Iyengar, Chase Audirsch, R. Shepherd, and A. Diaz Artiles. "SmartSuit: Next generation Spacesuit for Planetary Exploration" (abstract + poster) In: *2020 NASA Human Research Program Investigators' Workshop*, Galveston, TX, January 27-30, 2020.
5. A. Diaz Artiles and R. Kobrick. "Health in Space Series: State of the Art Space Suit Design" (invited technical talk). Space Medicine and Life Sciences, Space Generation Advisory Council (SGAC), 6 February, 2020 (online): : https://www.youtube.com/watch?v=sxbBPl1BR5o&fbclid=IwAR3ompsI5JE-0shlzRO3tcRoEES2uESlUc87XQ_K4B4uGA3EhFyuSjo0iv8
6. A. Diaz Artiles (featuring SmartSuit) and Javid Bayandor. "From Science Fiction to Science Fact". Museum of Science + Industry, Chicago, 11 April, 2020.
7. L. Kluis, N. Keller, H. Bai, N. Iyengar, Chase Audirsch, R. Shepherd, and A. Diaz Artiles. "SmartSuit: An advance Planetary Spacesuit". Submitted to the *50th International Conference of Environmental Systems,* Lisbon, Portugal, 12-16 July 2020.

Podcasts:

- Podcast The Wire: The Future of Spacesuits:https://engineering.tamu.edu/news/2019/10/podcast/the-wire-future-of-spacesuits.html
- Podcast Huffiness Institute (Podcast Friday with Dr. Ana Artiles - Aerospace Engineer & Space Flight Researcher): https://huffinesinstitute.org/Podcasts/ArticleID/1983/264-Video-Podcast-Friday-with-Dr-Ana-Artiles-Aerospace-Engineer-Space-Flight-Researcher
- Podcast Bonus Bites: From one small step to the future of space exploration (featuring Dr. Ana Diaz Artiles): https://engineering.tamu.edu/news/2019/12/podcast/bonus-bytes-from-one-small-step-to-the-future-of-space-exploration-featuring-dr-ana-diaz-artiles.html

## 8.2 Poster NASA Human Research Program Investigator's Workshop 2020

# Smartsuit: Next Generation Spacesuit For Planetary Exploration

**Logan Kluis[1] (kluisl@tamu.edu), Nathan Keller[2], Hedan Bai[3], Narahari Iyengar[3], Robert Shepherd[3], Ana Diaz Artiles[1] (adartiles@tamu.edu)**
1. Department of Aerospace Engineering, Texas A&M University 2. Department of Health and Kinesiology, Texas A&M University 3. Cornell University

organic robotics lab

NIAC NASA Innovative Advanced Concepts

AEROSPACE ENGINEERING Bioastronautics and Human Performance

## Soft-Robotic Elements

**Figure 1:** When the soft-robotic actuator is pressurized and expands, the knee is flexed. The actuator is shown unpressurized [A] and Pressurized [B].

Pressurization of spacesuits creates increased torques on joints during Extra-Vehicular Activities (EVAs). By implementing soft-robotic actuation, mission performance can be improved on two fronts:

1. Reduction of torque required from astronauts
2. Addition of mechanical counter pressure to decrease prebreathe times and gas pressure

### Modeling Spacesuit Torques and Robotic Actuators

- Extravehicular Mobility Unit (EMU) joint torques can be integrated into biomechanical simulations[2] (e.g. walking motion in OpenSim)
- Information on the net joint moments gives insight into the required torque needed from the soft-robotic actuators and the predicted improvements in metabolic rates

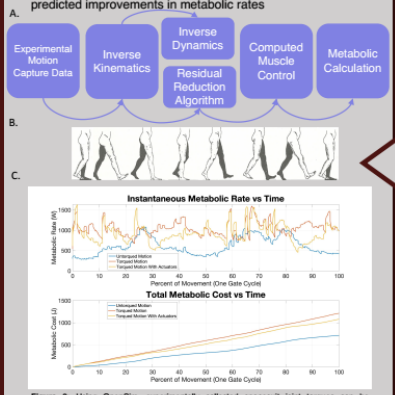


**Figure 2:** Using OpenSim, experimentally collected spacesuit joint torques can be integrated into simulated motions such as walking. The computed forces and torques from inverse dynamics can be used to estimate muscle force, activation, and metabolic cost. A flow chart of the process is shown [A]. The walking motion used in simulations is visually represented [B]. One gate cycle begins and ends with the right foot in the mid-swing phase. Instantaneous metabolic rate and total metabolic cost for a walking motion with and without torques and actuators is shown in [C].

Implementing 10Nm Torque actuators to the ankles, knees, and hips results in a 15% reduction in metabolic consumption.

### Testing Prototype Actuators

- Our first prototype was tested using a 4-point bending framework to characterize the relationship between actuator angle, torque generated, and pressure needed to actuate.
- The unique design of the actuators results in limited torque output at higher angles.

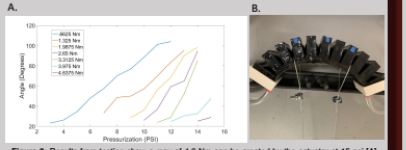


**Figure 3:** Results from testing show a max of 4.6 Nm can be created by the actuator at 15 psi [A]. The setup used for testing is shown in [B].

## Overview

As humans expand our need to evolve to other planets, spacesuits will need to be improved to reduce risk, fatigue, and metabolic expense. Current spacesuits have limited interaction with the environment and punctures may result in catastrophic failures. The SmartSuit will enhance multiple aspects of modern day suits, such as:

- Mobility & Comfort
- Reusability, Reparability & Safety
- EVA Preparation and Duration Time

**Improvements are facilitated by the integration of three technological innovations:**

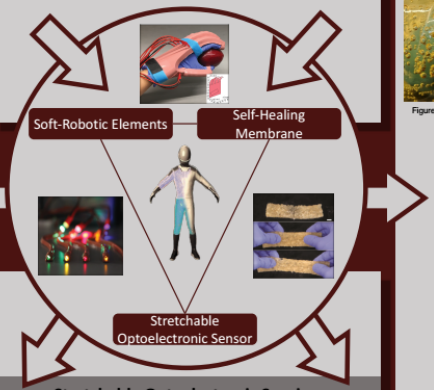


## Stretchable Optoelectronic Sensing

The stretchable sensors serve to provide proprioception (e.g. motions of bending and stretching) and exteroception (e.g. external pressure) sensing that provides feedback to astronauts regarding suit performance during EVA and detect damage to provide warning for potential oxygen leakage.

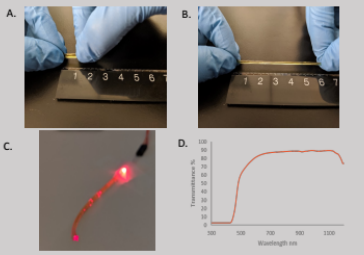


**Figure 5.** The material must be stretchable and the sPUU is capable of stretching to over 500% without breaking and stretches back with good resilience [A] [B]. The sPUU also meets the light propagation specification through approximately 90% transparency with 1.5mm thickness.

## Self-Healing Membrane

The membrane is made of a self-healing polyurethane urea elastomer (sPUU), with soft segments composed of poly(tetramethylene glycol) (PTMEG, Mw=1000) and isophorone diisocyanate (IPDI), and hard segment of bis(4-hydroxyphenyl) disulfide (S-S). sPUU self-heals intrinsically with the dynamic disulfide covalent bond (S-S) through disulfide metathesis[3]. Compared to other self-healing mechanisms such as extrinsically self-healing materials previously explored on spacesuits[4], this intrinsic healing mechanism does not require any external reagents nor special conditions (heat/light) to initiate the healing process. Therefore, it can self-heal under all conditions, which enhances the safety of astronauts by protecting them from depressurization events.


Figure 4. Self-healing property of sPUU: 2mm deep cut self-heals almost completely in 1 minute, and self-heals completely in 12 hours (tests completed at room temperature )

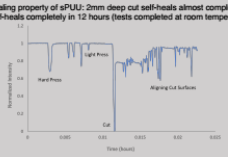


Figure 5

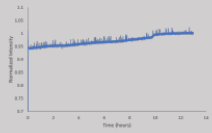


Figure 6

The tested capabilities of the optoelectronic sensors in the sPUU membrane are shown in Figures 5 and 6. The sensors were able to detect pressure at varying degrees of force and a cut (both indicated in Figure 5). The intensity is partially recovered after the blade is removed. At this stage we manually aligned the cut surfaces together which returned the intensity back to 94% of the original signal. The damaged sensor was then observed at room temperature for 12 hours without any intervention. Figure 6 shows the sensor signal fully recovered to the undamaged level (normalized intensity = 1 after healing) as the sPUU self-healed in 12 hours.

## References

1. Diaz, A., Anderson, A., Kracik, M., Trotti, G., and Hoffman, J. (2012). Development of a Comprehensive Astronaut Spacesuit Injury Database. 63rd International Astronautical Congress, 2012, pp. 1–9.
2. Diaz, A., Newman, D. (2014). Musculoskeletal Human-Spacesuit Interaction Model. IEEE Aerospace Conference Proceedings 2014–June, 2014
3. Li, S., Tu, Y., Bai, H., Hibi, Y., Wiesner, L., Pan, W., Wang, K., Giannelis, E. and Shepherd, R. (2019). Simple Synthesis of Elastomeric Photomechanical Switches That Self-Heal. Macromolecular Rapid Communications, 40(4), p.1970009.
4. Saemobilus.sae.org. (2019). Self-Healing Technology for Gas Retention Structures and Space Suit Systems (2007-01-3211 Technical Paper)- SAE Mobilus. [online] Available at: https://saemobilus.sae.org/content/2007-01-3211/
5. Kim, S., Jeon, H., Shin, S., Park, S., Jegal, J., Hwang, S., Oh, D. and Park, J. (2018). Self-Healing Materials: Superior Toughness and Fast Self-Healing at Room Temperature Engineered by Transparent Elastomers (Adv. Mater. 1/2018). Advanced Materials, 30(1), p.1870001.



NIAC NASA Innovative Advanced Concepts

NASA

## 8.3 Selected News & Media Coverage

Texas A&M Today:

TEXAS A&M TODAY | SCIENCE & TECH | BUSINESS & GOVERNMENT | ARTS & HUMANITIES | CULTURE & SOCIETY | CAMPUS LIFE | HEALTH & ENVIRONMENT

Subscribe | Press Room

SCIENCE & TECH

# New SmartSuit Promises A Better Fit For Astronauts

*The SmartSuit design concept developed by Texas A&M's Dr. Ana Diaz Artiles incorporates soft robotics technology, lending better mobility and dexterity to astronauts.*

By Jan McHarg, Texas A&M University College of Engineering • APRIL 17, 2019

SHARE 23 SHARES

NASA's Management and Development of Spacesuits audit in 2017 noted that NASA continues to manage an array of design and health risks associated with the current suit worn in space, the Extravehicular Mobility Unit (EMU). A new intelligent hybrid SmartSuit design proposed by Dr. Ana Diaz Artiles from Texas A&M University has the potential to solve some of these issues.

The SmartSuit, a spacesuit designed in mind for planetary exploration of the Moon and Mars, incorporates soft robotics technology, lending better mobility and dexterity to the astronauts and allowing them to better interact with their surroundings during extravehicular activities (EVA). The technology was recently selected for a NASA Innovative Advanced Concepts (NIAC) Phase I grant.

The suit will incorporate a soft and stretchable self-healing skin located in the outer layer that not only protects the astronaut but also collects data through integrated, transparent sensors embedded in the membrane. These sensors are capable of visually displaying environmental and membrane structural information, providing visual feedback to the wearer about the surroundings.

The current suits worn when working outside of the International Space Station (the EMU) are highly-pressurized with no robotic assistance, requiring astronauts to work against the suit and use their strength to move.

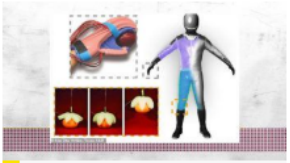

The SmartSuit design concept developed by Dr. Ana Diaz Artiles will incorporate a soft and stretchable self-healing skin located in the outer layer.

*Photo courtesy of Dr. Ana Diaz Artiles*

"The spacesuit is like a big balloon. When you try to bend your leg it has this tendency to come back to the natural position, so you're fighting against the suit every time you try to make a move," says Diaz Artiles, adding that this can lead to astronaut fatigue, as well as musculoskeletal injuries and discomfort.

The soft robotic technology proposed can increase human performance during EVA, improving mobility within the suit and allowing for a full range of movements. The sensors embedded in the skin of the suit will allow for an enhanced interaction with the environment during EVA, permitting astronauts to actually "feel" rocks when exploring the Mars surface.

Another benefit to the soft robotic layer, when extended over the entire body surface, is the generation of a continuous mechanical counterpressure. Decompression sickness (DCS) is an important consideration during EVA operations. To prevent DCS during exposure to spacesuit pressures, astronauts pre-breathe pure oxygen prior to depressurization to wash out nitrogen from body tissue. The duration of this pre-breathing can be as long as four hours.

With some pressure being provided by the soft robotic layer, the gas-generated pressure in the suit could be lowered, which in turn could result in a significant reduction in pre-breathing times necessary, dropping from four hours to as little as 90 minutes.

In addition, the self-healing membrane of the SmartSuit has the potential to protect an astronaut in the event of a puncture during an EVA on Mars surface, increasing astronaut safety during traverses. The stretchable optoelectronics embedded in the membrane will provide a means of monitoring spacesuit stress, helping to determine where failure in the suit is most likely to occur and notifying the astronaut if the self-healing membrane is severely damaged.

In the 2019 round, NIAC selected 12 projects for the Phase I awards, valued around $125,000. The Phase I studies are exploratory, nine-month projects that allow researchers to further develop their ideas. If the concept is awarded Phase II, the project will move forward with up to $500,000 more in funding for two years to advance the technology even further.

Diaz Artiles, associate professor in the Department of Aerospace Engineering, will lead the mission architecture work of this study, including a comprehensive biomechanical and human performance analysis.

Her co-investigator, Dr. Robert Shepherd, associate professor at Cornell University, will analyze material and mechanical metrics for manufacturing the SmartSuit and will also perform preliminary experimental validation of its core concepts.

Next Big Future:

## Next Generation Smartsuit Spacesuit with Soft Robotics

Brian Wang | June 14, 2019

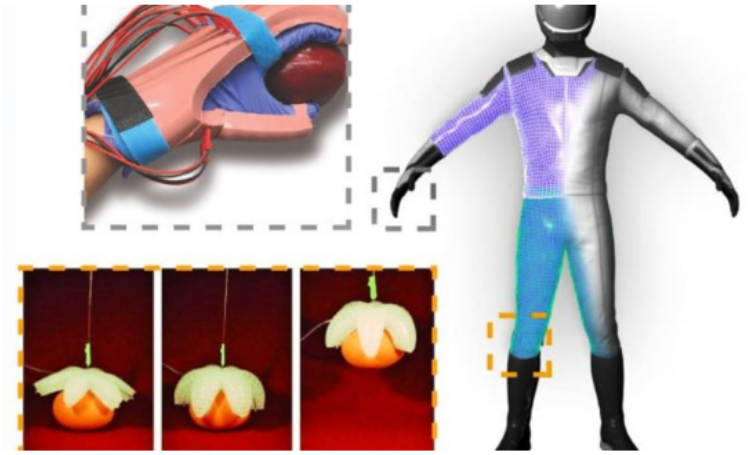

12

NASA NIAC has funded the development of a next-generation SmartSuit spacesuit which will use soft-robotics technology so astronauts can be more mobile and better interact with their surroundings.

The spacesuit will have a soft and stretchable self-healing skin (or membrane) located in the outer layer that not only protects the astronaut but also collects data through integrated, transparent sensors embedded in the membrane. These sensors are capable of visually displaying environmental and membrane structural information, providing visual feedback to the wearer about the surroundings.

The hybrid and intelligent spacesuit proposed will be designed with the philosophy of enhancing motion and dexterity, reparability and sensor integration to interact with the soundings and detect damage. The proposed hybrid technology adding full-body soft robotic elements to the gas-pressurized spacesuit will enable enhanced dexterity, increased comfort, and a feeling of normalcy that will facilitate both scientific and exploration operations on planetary missions like those expected for Mars' surface. Additionally, the soft-robotic layer has the potential to provide some level of mechanical counter pressure (MCP) to the wearer, thus decreasing the gas-operating pressure within the suit, therefore reducing the time needed for pre-breathing protocols while enhancing even more the mobility, which has a direct impact on the duration, metabolic cost, and fatigue associated with an EVA.

They expect the proposed spacesuit technology to reduce the numerous spacesuit-fit injuries and discomfort experienced by present astronauts due to the current highly pressurized spacesuits with no robotic assistance. The proposed spacesuit significantly improves on the state of the art in spacesuit design, addressing many issues in surface mobility, reparability and re-usability, safety, EVA preparation time, EVA duration time, and both physical and psychological fatigue. The Phase 1 effort constitutes advancement of this concept from TRL 1 to TRL 2.

The proposed project will investigate the trade-space of materials and sensor architectures, leading to design principles and sizing estimates of a candidate spacesuit. They propose to prove its feasibility and whether SmartSuit will achieve the science and exploration objectives articulated in the current Mars Design Reference Architecture 5.0. At the end of the phase I, they will outline the SmartSuit system design and concept of operations, including rationales for material, sensor, and display technology selection. It will also detail the layer breakdown and composition of such a suit. PI Diaz Artiles will lead the mission architecture work of this study, including a comprehensive biomechanical and human performance analysis. Co-I Shepherd will analyze material and mechanical metrics for manufacturing the SmartSuit and will also perform preliminary experimental validation of its core concepts (i.e. joint torques and MCP measurement, basic locomotion, relevant environmental sensing and display, and environmental stability).

Texas A&M Spirit Magazine – Fall 2019

## OUT-OF-THIS-WORLD SPACESUITS

An aerospace engineer at Texas A&M University is partnering with colleagues at Cornell University to transform the future of astronauts' spacesuits. Dr. Ana Diaz Artiles is investigating a new intelligent, hybrid SmartSuit to help resolve design and health risks associated with the current spacesuit, known as the Extravehicular Mobility Unit (EMU). The project is funded by the NASA Innovative Advanced Concepts Program.

The SmartSuit, designed for exploration of the moon and Mars, incorporates soft robotics technology and gives astronauts better mobility and dexterity during extravehicular activities. The suit includes a stretchable self-healing skin that not only protects the wearer in the event of puncture, but also collects data through integrated sensors in its membrane, providing visual feedback to astronauts about their surroundings. These sensors also allow for enhanced interaction with the environment, permitting astronauts to actually "feel" rocks and terrain.

The current EMU is highly-pressurized with no robotic assistance, causing astronauts to expend extra energy. "Today's spacesuit is like a big balloon," said Diaz Artiles. "Astronauts fight against the suit when they move, which can lead to fatigue, musculoskeletal injuries and discomfort." Before donning the EMU, astronauts must pre-breathe pure oxygen for up to four hours to avoid risking decompression sickness. The soft robotic technology of the SmartSuit is envisioned to provide a level of mechanical counterpressure so that astronauts would need to pre-breathe oxygen for as little as 90 minutes.